



PACIFIC EARTHQUAKE ENGINEERING RESEARCH CENTER

Reduced Uncertainty of Ground Motion Prediction Equations through Bayesian Variance Analysis

Robb Eric S. Moss

California Polytechnic State University
San Luis Obispo, California

Reduced Uncertainty of Ground Motion Prediction Equations through Bayesian Variance Analysis

Robb Eric S. Moss

Department of Civil and Environmental Engineering,
California Polytechnic State University, San Luis Obispo

PEER Report 2009/105
Pacific Earthquake Engineering Research Center
College of Engineering
University of California, Berkeley
November 2009

ABSTRACT

A ground motion prediction equation estimates the mean and variance of ground shaking with distance from an earthquake source. Current relationships use regression techniques that treat the input variables or parameters as exact, neglecting the uncertainties associated with the measurement of shear wave velocity, moment magnitude, and site-to-source distance. This parameter uncertainty propagates through the regression procedure and results in model uncertainty that overestimates the inherent variability of the ground motion. This report discusses methods of estimating the statistical uncertainty of the input parameters, and procedures for incorporating the parameter uncertainty into the regression of ground motion data using a Bayesian framework. This results in a better measure of the uncertainties inherent in the phenomena of ground motion attenuation and a reduced and more accurately defined model variance. A reduced model variance translates to a better constrained estimate of ground shaking for projects designed for rare events or events toward the tail of the distribution.

ACKNOWLEDGMENTS

This work was supported in part by the Pacific Earthquake Engineering Research Center (PEER) and the United States Geological Survey (USGS) National Earthquake Hazards Reduction Program (NEHRP). PEER's funding was from the California Department of Transportation (Caltrans), the California Energy Commission (CEC), and Pacific Gas and Electric Company (PG&E), by means of the PEER Lifelines project task number 1N01. Funding from USGS, Department of Interior, was through NEHRP award number 06HQGR0044. Any opinions, findings, and conclusions or recommendations expressed in this material are those of the author and do not necessarily reflect those of the funding agencies.

Thanks to Prof. Armen Der Kiureghian for providing the fundamental ground work that led to this study. Thanks to Alison Faris for her assistance in troubleshooting the Bayesian regression algorithm.

The following researchers graciously provided data for the V_{S30} portion of the study: Ron Andrus, David Boore, Leo Brown, John Louie, Glenn Rix, Bill Stephenson, Carl Wentworth, and Jianghai Xia. Discussions with Adrian Rodriguez-Marek, Ken Campbell, and Yousef Bozorgnia were helpful in sorting out some of the details related to ground motion prediction equations and the various regression steps used to fit a model to the data.

Thanks to Gail Atkinson, Rob Williams, and an anonymous reviewer who provided input that helped improve the BSSA paper on the V_{S30} component of the study.

The PEER review panel provided needed direction and guidance throughout the research timeline. Tom Shantz, Brian Chiou, Yousef Bozorgnia, and Norm Abramson are thanked for their valuable input.

CONTENTS

ABSTRACT.....	iii
ACKNOWLEDGMENTS	iv
TABLE OF CONTENTS	v
LIST OF FIGURES	vii
LIST OF TABLES	xi
1 INTRODUCTION	1
2 CONCEPTUAL AND MATHEMATICAL FORMULATION	3
2.1 Model Uncertainty	3
2.2 Measurement Error	4
2.3 Statistical Uncertainty	4
2.4 Parameter Estimation through Bayesian Updating	4
2.5 Likelihood Function	6
3 FEASIBILITY STUDY	9
4 QUANTIFYING PARAMETER UNCERTAINTY	13
4.1 Thirty Meter Shear Wave Velocity (V_{S30})	13
4.1.1 Intra-Method Variability	15
4.1.2 Inter-Method Variability	20
4.1.3 Variability of V_{S30} correlated Geologic Units.....	31
4.1.4 Application of V_{S30} Uncertainty Point Estimate	34
4.1.5 Spatial Variability of V_{S30} Measurements.....	36
4.1.6 V_{S30} Variance Results and Conclusions	38
4.2 Moment Magnitude (M_W)	39
4.3 Distance (R)	41
5 IMPLEMENTATION AND RESULTS	47
5.1 Chiou and Youngs Attenuation Model	47
5.2 Approximate Solutions.....	51
5.2.1 First-Order Second-Moment Method.....	51
5.2.2 Monte Carlo Simulations	53

5.3	Other Ground Motion Prediction Equations	54
5.4	Impact of Results	55
6	SUMMARY AND CONCLUSIONS.....	59
	REFERENCES.....	61
	APPENDIX	

LIST OF FIGURES

Fig. 3.1	Pie chart showing relative contribution of 30 m shear wave velocity (V_{S30}) and Joyner-Boore distance (R_{jb}) measurement uncertainty to overall model intra-event uncertainty.....	10
Fig. 3.2	Pie chart showing relative contribution of moment magnitude (M_w) measurement uncertainty to overall model intra-event uncertainty.	11
Fig. 3.3	Comparison plot of ground motion prediction using “classic” regression with exact parameters versus Bayesian regression that incorporates parameter uncertainty. Black curves are from Boore et al. (1997), red curves from this study. Plus/minus one standard deviation curves are shown as dashed lines.....	12
Fig. 4.1	Combined results from various studies showing intra-method variability.	20
Fig. 4.2	Results from Asten and Boore (2005) showing nine VS30 test methods with respect to suspension logging.....	23
Fig. 4.3	Combined results of comparison studies showing inter-method variability for SASW and MASW.	24
Fig. 4.4	Combined results of comparison studies showing inter-method variability for reflection/refraction and ReMi methods.	25
Fig. 4.5	Difference between V_{S30} and V_{S5-30} are shown to determine if near-surface effects are cause of bias between invasive and non-invasive methods. Diamonds are VS30 data and circles V_{S5-30} data, from sites presented in Brown et al. (2002). Linear trend lines show almost parallel slopes indicating no bias can be attributed to near-surface effects on invasive methods based on this hypothesis.....	26
Fig. 4.6	Comparison of V_{S30} from suspension logging and downhole or SCPT at six sites. Brown et al. (2002) presented suspension logging and downhole data for each site. Asten and Boore (2005) presented one site with suspension logging, SCPT, and downhole seismic.....	29
Fig. 4.7	Linear regression of invasive versus non-invasive; all data from Fig. 4.3. Statistics shown in upper left corner.....	30
Fig. 4.8	Mean and coefficient of variation of V_{S30} for each of 19 generalized geologic units presented in Wills and Clahan (2004).....	32
Fig. 4.9	Predicted versus measured V_{S30} from Wills and Clahan (2004).....	33

Fig. 4.10	Linear regression fit to trend of increasing coefficient of variation with increasing 30 m shear wave velocity for V_{S30} correlated geologic units. Mean and ± 1 standard deviation lines are shown. Regression results in the upper left corner.	34
Fig. 4.11	Spatial variability of SCPT and SASW measured V_{S30} for an 8 km stretch in the Bay Area, from (Thompson et al. 2007)	37
Fig. 4.12	Plot of Thompson et al. (2007) SASW data fit with exponential model.	38
Fig. 4.13	Moment magnitude versus standard deviation of moment magnitude. Several lines have been fit to data, all showing a general decrease of variance with an increase in magnitude.	40
Fig. 4.14	Coefficient of variation of each distance metric with respect to Joyner-Boore, R_{jb} , distance for different magnitudes, and distance bin of 5–15 km (after Scherbaum et al. 2004).	45
Fig. 4.15	Nominal or mean trend of the coefficient of variation of distance for various distance metrics, magnitudes, and distance bin of 5–15 km, with a polynomial fit for estimation purposes.	46
Fig. 5.1	Plot of V_{S30} versus natural log of spectral acceleration showing Bayesian regression duplicating “classic” regression with Chiou and Youngs (2008) model as limit-state function for period of 0.01 sec (PGA).	49
Fig. 5.2	Percent decrease in standard deviation of $\ln(SA)$ for different spectral periods. Database average V_{S30} measurement uncertainty taken into account was $COV \approx 27\%$. Error bars show convergence tolerance as a standard deviation of results for each spectral period.	50
Fig. 5.3	Plot showing 3.0 sec period results. Decrease of 9% in standard deviation of $\ln(SA)$ is realized by taking into account V_{S30} measurement uncertainty using Bayesian regression.	51
Fig. 5.4	First-order second-moment (FOSM) variance analysis results. These results compare favorably with Bayesian regression results, lending support to results of both methods and confirming that simplified methods provide reasonable results.	51
Fig. 5.5	Monte Carlo (MC) simulation results with respect to FOSM and Bayesian regression results. All three methods show similar general trends.	54

Fig. 5.6	Chiou and Youngs (2008) probability density function predictions for PGA and 3.0 sec period, given earthquake, distance, and site conditions compared to probability density function that accounts for parameter uncertainty in V_{S30} . Difference in 1 sigma and 2 sigma results demonstrates the impact of variance analysis on ground motion prediction of rarer events.	57
Fig. A1	Bayesian regression results that mimic “classic” regression results using Ang and Tang E71 example. Median and plus and minus standard deviation lines are shown with data.	A-7
Fig. A2	Bayesian regression results where parameter uncertainty of depth is taken into account. Reduced model uncertainty is realized by including parameter uncertainty.	A-7

LIST OF TABLES

Table 3.1	Intra-event uncertainty.....	9
Table 3.2	Inter-event uncertainty.....	10
Table 4.1	List of comparative studies used to quantify intra-method variability.....	16
Table 4.2	List of blind studies used to quantify inter-method variability.....	21
Table 4.3	Description of geologic units shown in Fig. 4.8 (after Wills and Clahan 2004).	31
Table 4.4	Summary of contributors to distance uncertainty.....	43

1 Introduction

Recent probabilistic seismic hazard assessments of proposed nuclear sites have shown that long-return period (i.e., rare) events are predicted to produce ground motions that are unreasonably high. There are a number of reasons for these high predictions, one being that measurement uncertainty from each of the independent variables in the ground motion prediction equation is translated through to the dependent variable. For rare events a large variance results in large ground shaking estimates that are not necessarily statistically accurate. This report describes research into measurement uncertainty and its impact on the variance of ground motion prediction equations.

The most common statistical method for developing a ground motion prediction equation is univariate regression on a database using a fixed-effects or random-effects model (Abrahamson and Silva 1997; Boore et al. 1997; Campbell and Bozorgnia 2003). This methodology assumes that the input parameters are exact. There exists, however, measurement uncertainty in the input parameters. Thirty meter shear wave velocity (V_{S30}), moment magnitude (M_W), and site-to-source distance (R) are all subject to some form of measurement uncertainty. For instance, the moment magnitude of a particular seismic event is calculated using a non-unique inversion process resulting in a specific amount of uncertainty. By quantifying the measurement uncertainty of the input parameters and accounting for this uncertainty in the regression procedure, a reduced and more accurate estimate of the model variance can be found. This better estimate of the model variance is also more representative of the inherent variability of the attenuation phenomena. A Bayesian framework, used in this study for model fitting that is analogous to univariate regression, allows for the treatment of input parameters as inexact, and provides the mathematical flexibility to use any type of functional model form (Der Kiureghian 2000; Gardoni et al. 2002; Moss et al. 2003).

This report describes the background, basis, and results of incorporating parameter uncertainty into the ground motion prediction equations. The research is presented in the chronological order that it was conducted. Chapter 2 presents the conceptual and mathematic formulation used for Bayesian regression. Chapter 3 describes a feasibility study that was conducted early in this research to demonstrate that this method works, and shows reduced model variance results based on rough estimates of the parameter uncertainty. The Boore et al. (1997) attenuation relationship was used for the basis function of the feasibility study. Chapter 4 provides details on methods of statistically estimating the parameter uncertainty of each of the input parameters. Most research to date has focused on 30 m shear wave velocity (V_{S30}) because it is a sensitive input parameter. Chapter 5 describes the implementation of Bayesian regression and V_{S30} uncertainty using the NGA (Next Generation Attenuation) model by Chiou and Youngs (2006). A summary and conclusions are presented in Chapter 6. The Appendix contains a basic version of the Matlab code that was used to perform the Bayesian regression analyses.

2 Conceptual and Mathematical Formulation

The conceptual and mathematical formulation of the model fitting found in this study uses a Bayesian-type regression procedure that was first outlined for the application of ground motion prediction equations in Moss and Der Kiureghian (2006). The procedure is regression in the sense that a minimized error is found between the data and a best-fit line; however the independent variables or input parameters are treated as inexact, possessing statistical uncertainty due to some form of measurement error.

The prediction of strong ground motion uses a univariate-type model. It is univariate because only one quantity of interest is to be predicted from a set of measurable variables $x=(x_1, x_2, \dots, x_n)$. The quantity of interest in this case is the spectral acceleration. The general univariate model can be written as,

$$Z = Z(x, \Theta) \quad (2.1)$$

where Θ denotes a set of model parameters used to fit the model to the observed data. In this study two models, based on ground motion prediction equations in the literature, will be used. The generalized univariate model can then be written as

$$Z(x, \Theta) = \hat{z}(x, \Theta) + \varepsilon \quad (2.2)$$

where $\hat{z}(x, \Theta)$ is the selected ground motion prediction equation and ε is a random normal variate with zero mean and unknown standard deviation that is the model error term. Aleatory uncertainty is found in the measured variables x and partly in the error term ε . Epistemic uncertainty is found in the model parameters Θ and partly in the model error term ε .

2.1 MODEL UNCERTAINTY

In this model formulation the error term ε captures the imperfect fit of the model to the data. The imperfect fit may be due to inexact model form or due to missing variables. The missing

variables can be considered inherently random and that portion of the model error term is aleatory uncertainty. The portion of the model error term that is from the inexact model form is epistemic uncertainty.

2.2 MEASUREMENT ERROR

Measurement error tends to comprise a large portion of the epistemic uncertainty in geoscience problems. This uncertainty comes from imprecise measurement of the variables $x=(x_1, x_2, \dots, x_n)$. These measurement errors are treated as statistically independent, normally distributed random variables with zero mean (assuming unbiased measurement errors) and quantifiable standard deviation. The errors are incorporated as $x_i = \hat{x}_i + e_{xi}$ where $\hat{x}_{i, xi}$ is the measured value and e_{xi} is the measurement error.

2.3 STATISTICAL UNCERTAINTY

The size of the sample n will influence the accuracy of the model parameters Θ . The larger the sample size, the less epistemic uncertainty introduced into the model parameters. In this case, there is a limited amount of ground motion recordings for model fitting.

2.4 PARAMETER ESTIMATION THROUGH BAYESIAN UPDATING

A Bayesian framework is used to estimate the unknown model parameters, the objective of regression. The Bayesian approach is useful because it incorporates all forms of uncertainty related to the problem of ground motion prediction into the regression analysis.

Bayes's rule is derived from simple rules of conditional probability, yet the simplicity portends little of the power of the Bayesian technique. Bayes's rule can be written as (Box and Tao 1992):

$$f(\Theta) = c \cdot L(\Theta) \cdot p(\Theta) \quad (2.3)$$

where; $f(\Theta)$ is the posterior distribution representing the updated state of knowledge about Θ , $L(\Theta)$ is the likelihood function containing the information gained from the observations of x ,

$p(\Theta)$ is the prior distribution containing *a priori* knowledge about Θ , and $c = [\int L(\Theta) \cdot p(\Theta) \cdot d(\Theta)]^{-1}$ is the normalizing constant.

The likelihood function is proportional to the conditional probability of the observed events, given the values of Θ . The likelihood function incorporates the objective information that in this case are the measurements of earthquake ground motions. The prior distribution can include subjective information known about the distributions of Θ . The posterior distribution incorporates both the objective and subjective information into the distributions of the model parameters. The process of performing Bayesian updating involves formulating the likelihood function, selecting a prior distribution, calculating the normalizing constant, and then calculating the posterior statistics.

The prior distribution tends to be the most controversial issue for detractors of Bayesian methods. Box and Tiao (1992) have shown that the use of a non-informative prior distribution can lead to an unbiased, data-driven estimate of the model parameters. A non-informative prior distribution allows the data, through the likelihood function, to dominate the posterior distribution, thereby minimizing the role of the subjective information. A non-informative prior distribution, by definition, has no effect on the shape of the posterior distribution and is used when no prior information about the parameters is available. Gardoni et al. (2002) discuss that for a univariate model where the unknown parameters Θ are composed of the coefficients in a linear expression in addition to the model error term ε , the non-informative prior distribution simplifies to the reciprocal of the vector containing the standard deviations of the coefficients and the model error term:

$$p(\Theta) \equiv p(\sigma) \propto \frac{1}{\sigma} \quad (2.4)$$

The mean vector M_Θ and covariance matrix $\Sigma_{\Theta\Theta}$ can be calculated from the posterior distribution of Θ . Computation of these statistics and the normalizing constant is non-trivial, requiring multifold integration over the Bayesian kernel. Importance sampling, a sampling algorithm as described in Gardoni (2002) was used to efficiently perform these calculations.

2.5 LIKELIHOOD FUNCTION

As defined above the likelihood function is proportional to the conditional probability of observing a particular event given values of Θ . In order to formulate the likelihood function a limit state must be defined to provide a threshold for defining the probability of observation.

To demonstrate the formulation of the likelihood function, the ground motion prediction equation from Boore et al. (1997) is used as the basis because it is relatively simple in mathematical form; it is used subsequently in this study for the feasibility study. The function form is

$$\log(Y) = \theta_1 + \theta_2(M_w - 6) + \theta_3(M_w - 6)^2 - \theta_4 \ln(\sqrt{R_{jb}^2 + \theta_5^2}) - \theta_6 \ln(V_s / \theta_7) \quad (2.5)$$

where Y represents the spectral acceleration value, M_w is the moment magnitude, R_{jb} is the Joyner-Boore distance, V_s is the shear wave velocity in the upper 30 m, and the θ 's are the model parameters. Boore et al. (1997) determined the parameters of this model using what will be called in this discussion “classic” regression with a two-step procedure.

To present this prediction equation as a limit-state function, the equation is rearranged to describe the most likely location of a threshold given a value of Θ . This limit state would be where the threshold lies at the zero mean of the error term at a value of Z_i for a given x_i . This thereby minimizes the error on each side of the threshold at that point. From Equation 2.2, $Z_i = \hat{z}(x_i, \theta) + \varepsilon_i$ or $\varepsilon_i = g_i(\theta)$ where $g_i(\theta) = Z_i - \hat{z}(x_i, \theta)$ and ε_i is the model error term at the i^{th} observation. The attenuation relationship of Boore et al. (1997), shown in Equation 2.5, then becomes

$$g(\Theta) = \log(Y) - [\theta_1 + \theta_2(M_w - 6) + \theta_3(M_w - 6)^2 - \theta_4 \ln(\sqrt{R_{jb}^2 + \theta_5^2}) - \theta_6 \ln(V_s / \theta_7)] \quad (2.6)$$

The likelihood function for the problem of the ground motion prediction equation is the product of the probabilities of observing n values with the limit state collocated with the zero mean of the error term. Given exact measurements and statically independent observations, the likelihood can be written as

$$L(\theta, \sigma_\varepsilon) \propto P \left[\bigcap_{i=1}^n \{g_i(\theta) = \varepsilon_i\} \right] \quad (2.7)$$

where σ_ε is the standard deviation of the error term ε . Given that ε is a standard normal variate, Equation 2.7 can be written as

$$L(\theta, \sigma_\varepsilon) \propto \prod_{i=1}^n \left\{ \frac{1}{\sigma_\varepsilon} \varphi \left[\frac{g_i(\theta)}{\sigma_\varepsilon} \right] \right\} \quad (2.8)$$

where φ is the standard normal distribution function. When measurement errors are considered, the likelihood function becomes

$$L(\theta, \sigma_\varepsilon) \propto \prod_{i=1}^n \left\{ \frac{1}{\hat{\sigma}_\varepsilon(\theta, \sigma_\varepsilon)} \varphi \left[\frac{\hat{g}_i(\theta)}{\hat{\sigma}_\varepsilon(\theta, \sigma_\varepsilon)} \right] \right\} \quad (2.9)$$

The above formulation was used to estimate the statistics of the model parameters, Θ , and the model error, ε , for a given functional form of the ground motion prediction equation and the given database. These estimated terms are analogous to the coefficients solved for using classic regression in Boore et al. (1997). The mean and standard deviations of the coefficients are used to define the predictive model.

3 Feasibility Study

A feasibility study using Boore et al. (1997) as the basis for the limit-state function was performed to examine the relative impact that Bayesian regression would have on a ground motion prediction equation. A Bayesian regression was initially performed without parameter uncertainty to duplicate the regression results of Boore et al. (1997). The Bayesian regression was then performed with prescribed amounts of measurement uncertainty as shown in Tables 3.1 and 3.2. The pie charts, Figures 3.1 and 3.2, show the relative contribution of the measurement error to the total inter- and intra-event error, respectively.

The reduction in model uncertainty is shown as a “best” estimate. The Bayesian regression produces results that are slightly non-unique because of the iterative nature of the solution algorithm. Importance sampling is used to perform the integration over the Bayesian kernel; the accuracy of the results is controlled by the allowable tolerance on the coefficient of variation (COV) of the posterior means. All results shown in the table are mean values with a COV on the mean of less than 25%, which is a reasonably accurate result for these purposes.

Table 3.1 Intra-event uncertainty.

Parameter	σ_e	% Decrease	Notes
Base case with no parameter uncertainty	0.486		duplicated Boore et al. (1997) results
V_{S30}	0.412	15%	average COV=15%
R_{jb}	0.403	17%	average COV=15%

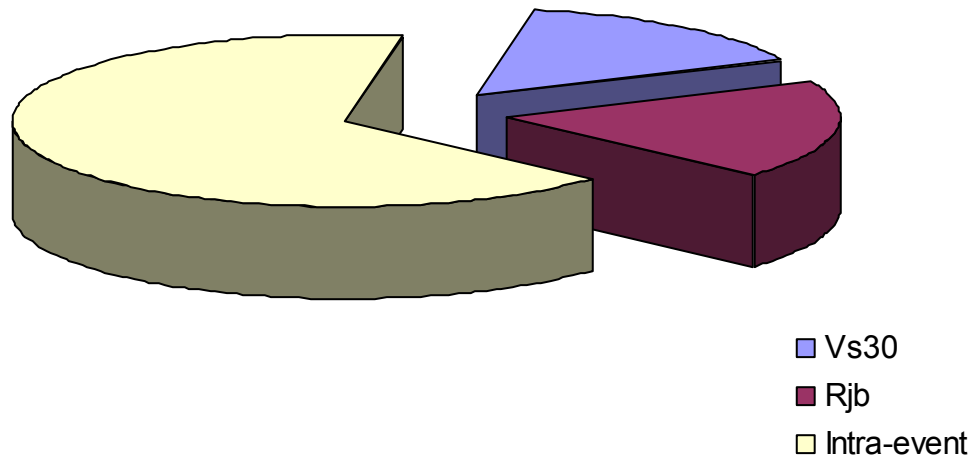


Fig. 3.1 Pie chart showing relative contribution of 30 m shear wave velocity (V_{s30}) and Joyner-Boore distance (R_{jb}) measurement uncertainty to overall model intra-event uncertainty.

Table 3.2 Inter-event uncertainty.

Parameter	σ_r	% Decrease	Notes
Base case with no parameter uncertainty	0.184		duplicated Boore et al. (1997) results
M_w	0.147	20%	logarithmic function (average stdev=0.1)

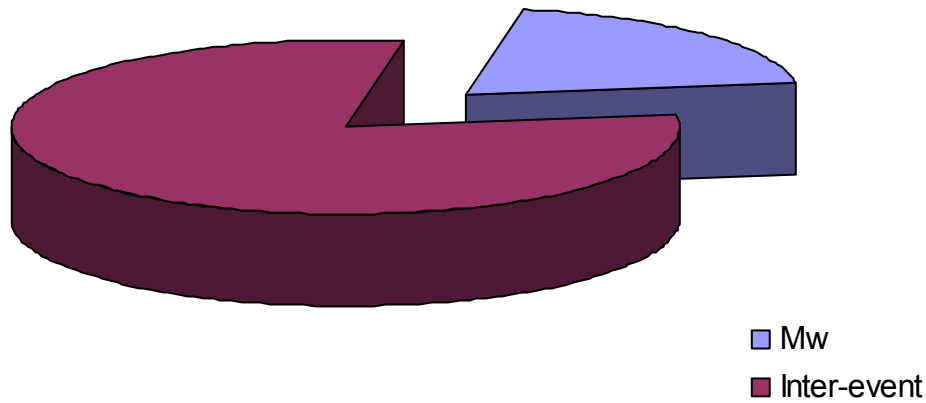


Fig. 3.2 Pie chart showing relative contribution of moment magnitude (M_w) measurement uncertainty to overall model intra-event uncertainty.

The model standard deviation in lognormal units reduces from 0.54 to 0.34 given the assigned parameter uncertainty from all three independent variables. This 37% reduction is shown in Figure 3.3 against the mean and standard deviation bounds of Boore et al. (1997). This feasibility study shows that by incorporating parameter uncertainty into the regression procedure, that a reduction in the uncertainty of the predictive equation can be realized, and this reduction is a function of the measurement error of the independent variables and the how these are related to the dependent variable through the limit-state function. The reduction demonstrates the relative contribution of measurement error to the total uncertainty versus inherent variability of the phenomena. The median prediction curve remains relatively constant, whereas the variance as defined by the standard deviation curves shows the influence of parameter uncertainty.

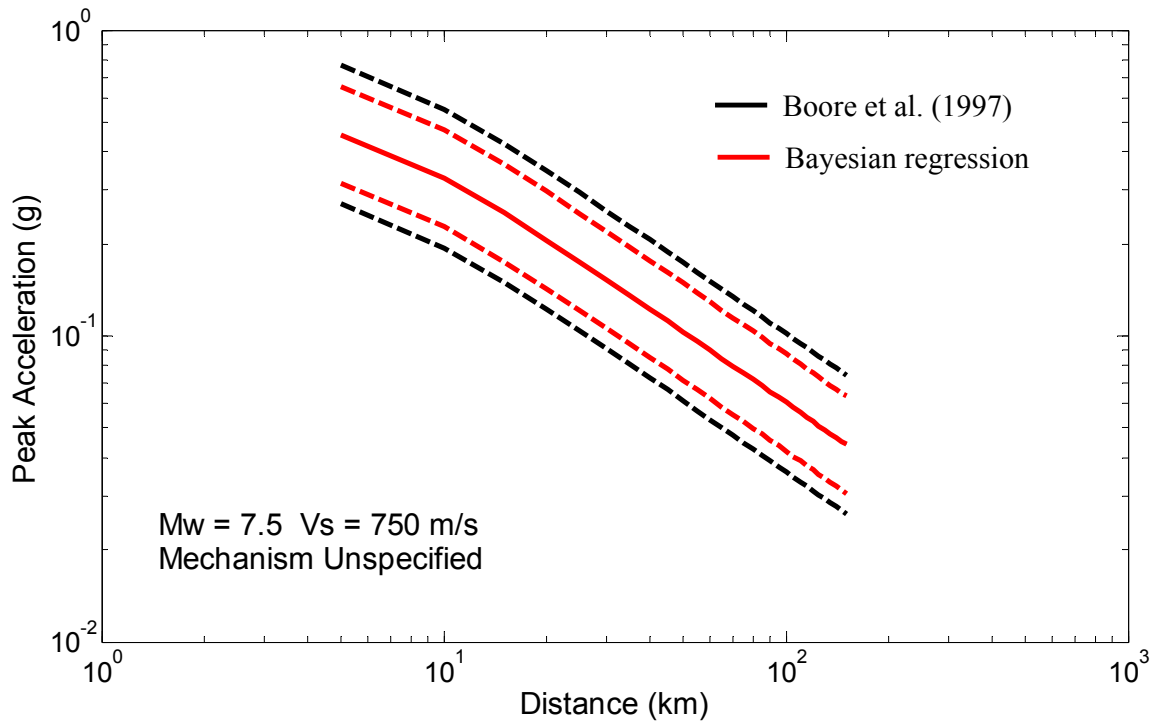


Fig. 3.3 Comparison plot of ground motion prediction using “classic” regression with exact parameters versus Bayesian regression that incorporates parameter uncertainty. Black curves are from Boore et al. (1997), red curves from this study. Plus/minus one standard deviation curves are shown as dashed lines.

4 Quantifying Parameter Uncertainty

Once the feasibility study confirmed that Bayesian regression would provide useful results, research effort was put into quantifying parameter or measurement uncertainty of the input variables; 30 m shear wave velocity, distance, and moment magnitude. Of these three, 30 m shear wave velocity received the most attention, as described in this chapter. Moment magnitude and distance (with its various metrics) require more investigations than what are presented here, but preliminary results are shown to document the progress.

4.1 THIRTY METER SHEAR WAVE VELOCITY (V_{S30})

Thirty meter shear wave velocity was thoroughly investigated as part of this research. The results have been published in Moss (2008) and are presented in a similar manner in this report. Measurement uncertainty is defined here as the epistemic uncertainty inherent in measuring some property such as shear wave velocity. This uncertainty can be composed of both a bias and an equally distributed error term. If measurement uncertainty is not quantified and treated appropriately, it propagates through an analysis and becomes lumped with other uncertainties into the model error. Uncertainty is additive in nature. The process of measuring some quantity is a summation of the different subprocesses that constitute the measurement.

By quantifying measurement uncertainty upfront it can be separated from inherent variability, thereby providing a more accurate estimate of the uncertainty associated with a phenomena. Measurement uncertainty, a type of epistemic uncertainty, can come in many forms, affecting both the accuracy and precision of a measurement (accuracy is how correct the measurement is, and precision is how repeatable the measurement is). Both are captured in this study, and a best estimate of the magnitude of the respective uncertainty is made based on existing data.

One difficulty in quantifying the measurement uncertainty associated with shear wave velocity is that although many methods can be used to measure or infer 30 m shear wave velocity, no single method provides what can be deemed an unbiased estimate. Two general method classes of measuring shear wave velocity of near-surface materials are (1) invasive and (2) non-invasive.

Invasive methods involve the measurement of the shear wave velocity from a bored or displaced hole with the source either at the surface or down the hole. Invasive types of shear wave velocity measurements include (a) seismic cone measurements (SCPT), where there is a seismometer in the cone and the source is generated at the ground surface; (b) standard downhole (DH) measurements, where a receiver is lowered into an open hole and the source is at the surface; (c) suspension logging, where a source and receiver are lowered into an open hole; and (d) cross hole, where there are two holes, one for the source and one for the receiver. The most commonly used invasive methods for measuring V_{S30} are seismic cone, standard downhole, and suspension logging. The seismic cone and the standard downhole methods are subject to increasing source to receiver distance with depth and become less accurate as a function of depth, number of soil layers or reflectors between the source and the receiver, and amplitude and frequency of the source with respect to ambient noise conditions. Suspension logging provides a constant source to receiver distance and therefore measures shear wave velocity on a fixed scale. Because of the short distance between source and receiver, the suspension measurements are usually smoothed or averaged over a depth range to better represent the shear wave velocity of the geologic material. The accuracy of suspension logging does not diminish with depth as it does with the seismic cone or standard downhole methods.

Non-invasive methods (using both active and passive sources) include SASW (spectral analysis of surface waves), MASW (multi-channel analysis of surface waves), f-k (frequency-wavenumber), SPAC (spatial autocorrelation), ReMi (refraction microtremor), reflection/refraction, HVSr (horizontal-vertical spectral ratio), SW (surface wave), and MAM (microtremor array) methods. Non-invasive methods are becoming more common for measuring V_{S30} . A number of methods are currently in use and being explored for future applications. The general procedure involves recording surface or body waves at the ground surface and resolving the subsurface structure or stiffness through forward or inverse modeling. Non-invasive methods were developed initially by the petroleum industry for exploring underground geologic structure and reservoirs, and seismologists for studying deep earth structure.

For the PEER (Pacific Earthquake Engineering Research Center) Strong Motion Database (<http://peer.berkeley.edu/smcat/>) at sites where no invasive or non-invasive measurements exist, V_{S30} has also been estimated based on surficial geology using a correlation between measured shear wave velocity and mapped surficial geology for a specific geologic environment. (Here strong motion sites refer to sites where seismographs have recorded ground motions from past earthquakes where the ground shaking intensity was high enough to result in structural and/or nonstructural damage.)

In this study, measurement uncertainty associated with V_{S30} are based on the shear wave velocity methods used for classifying strong motion sites in the PEER Lifelines NGA (Next Generation Attenuation) program: standard downhole, SCPT, suspension logging, SASW, and geologic-based estimates. This section presents the steps taken to quantify the apparent or observable V_{S30} measurement uncertainty for these methods based on existing field studies, and how to propagate that uncertainty mathematically. This research does not attempt to deconstruct and present the fundamental uncertainties involved in each specific test nor does it present new field test results toward that end.

4.1.1 Intra-Method Variability

In order to determine the measurement uncertainty of any individual test, multiple measurements need to be carried out at a single controlled location. To date, research to evaluate the measurement uncertainty of individual tests has been limited because of the amount of time and money required to run the tests and also because of the lack of appreciation of how measurement uncertainty can impact subsequent analyses. Table 1 lists the studies available in the literature (as of 6/2007) used to establish estimates of intra-method variability.

Table 4.1 List of comparative studies used to quantify intra-method variability.

Comparative Study	Methods Used
Xia et al. 2002	Downhole, Suspension log, MASW
Marosi and Hiltunen 2004	SASW
Martin and Diehl 2004	Simplified SASW, SASW, ReMi, Suspension log
Kayen 2005	SASW
Asten and Boore 2005	Downhole, SCPT, Suspension log, SASW, MASW, ReMi, SPAC, f-k, Reflect/Refract, HVSr
Thelen et al. 2006	Downhole, ReMi

Intra-method variability of non-invasive methods can be composed of the uncertainty associated with the inversion process for surface wave methods, curve-fitting procedures, waveform analyses, source differences, equipment differences, equipment fidelity, or spacing of instruments. These sources of uncertainty are lumped together so that a composite uncertainty measurement can be made.

Conceptually, intra-method variability does not include the spatial variability that is a function of the correlated change of shear wave velocity with distance. However in comparative studies it may be difficult to perform different tests at the same location. Thompson et al. (2007) presented some useful results showing spatial variability of shear wave velocity from SCPT and SASW data. Based on these results a distance of 10 m or less between measurements can have negligible results on the uncertainty; of course this depends on the depositional environment and the spatial heterogeneity of the soil.

Other sources of uncertainty to consider are the fundamental differences in the testing methods. A wave traveling from a surface source to a subsurface receiver is very different than a wave traveling from a source, reflecting off a boundary, and converting into a surface wave before being received. Treating the resulting V_{S30} values as the same may neglect how

anisotropy and shear wave polarization can impact the results. However there are currently insufficient data to separate out the different sources of method variability, so they are lumped together as a composite measurement uncertainty in this study.

Xia et al. (2002) evaluated uncertainty as a function of the number of recording channels, sampling interval, source offset, and receiver spacing using MASW. Important for this study was the multiple recordings made at two of the sites which produced a coefficient of variation (the coefficient of variation is equal to the standard deviation normalized by the mean; σ/μ or s/\bar{x}) of V_{S30} on the order of 1%. (Note that throughout this chapter the coefficient of variation will be used as a metric for measuring relative uncertainty because it allows for easy cross comparisons. The coefficient of variation values presented in this study have all been calculated from the source data.)

Marosi and Hiltunen (2004) presented a study that looked at the uncertainty associated with SASW measurements. Two sites were investigated and multiple SASW measurements were made at each site. It was found that there was low measurement uncertainty in the phase angle and phase velocity data, with a coefficient of variation typically around 2%, and that the data appeared to be normally distributed. When evaluating the resulting shear wave velocity data, the coefficient of variation was closer to 5%–10%, and exhibited an increase in uncertainty with depth and geologic complexity. These authors report that the increase in the uncertainty that occurs in the step to produce the shear wave data following generation of the phase information comes from picking the layer boundaries and fitting a dispersion curve to the data; “the inversion process appears to magnify the uncertainty in the dispersion data.” A shortcoming of this study is that the sites were explored to a maximum depth of just under 5 m with shear wave velocities in the range of 200–350 m/sec for both sites. Although this study can not be used to assess V_{S30} uncertainty, it is included here because it presents a good example of how multiple measurement field studies should be carried out, and it provides some useful general results.

Martin and Diehl (2004) describe a simplified SASW technique for determining a single value of V_{S30} as opposed to a full shear wave velocity profile. They compared the simplified technique to measurements from SASW, ReMi, and suspension logging. In this study the simplified SASW and standard SASW are treated as the same test with a variation in the procedure. The coefficient of variation for the simplified method is on the order of 6% from 103 different sites.

In an SASW course taught by Rob Kayen at the University of California, Davis, the same site was used by the students term after term for field measurements of shear wave velocity and V_{S30} (Rob Kayen personal communication, 2005 and 2006). This provided a useful data set to evaluate SASW intra-method variability, with the results indicating a coefficient of variation of V_{S30} of 4.7% with 6 independent measurements.

Asten and Boore (2005) carried out a large blind study at Coyote Creek that brought together many different researchers and different techniques for measuring shear wave velocity. For the purposes of intra-method variability there were 11 different V_{S30} estimates using SASW conducted by three different researchers, two MASW measurements by two different researchers, and three invasive measurements (downhole, SCPT, and suspension log) by three different researchers. Particularly useful are the SASW tests because of the large number of measurements with different techniques and different researchers, with an average coefficient of variation of V_{S30} of 4.8% with 11 measurements.

Thelen et al. (2006) performed ReMi cross sections through areas of the Los Angeles basin. To evaluate bias that may be due to forward modeling, the group had three separate analysts perform the data analysis and then compared the resulting V_{S30} estimates. This provided a well-constrained measurement of epistemic uncertainty with the resulting coefficient of variation ranging from 2 to 14% from 3 cases. The ReMi measurements were approximately within a few hundred meters from the existing downhole measurements and therefore were not used to assess inter-method variability.

Based on this literature review and discussions with various researchers, intra-method variability of SASW comes from the following:

- a small amount from phase angle and phase velocity data;
- a small amount from array length vs. frequency sweep observed as the variability of the dispersion curves;
- a greater amount that is a function of the inversion process, picking the layer depths, the number of layers, the water table location, the Poisson ratio;
- some amount from the lithology, non-horizontal bedding, other non-uniform subsurface conditions;
- some amount as a function of the equipment fidelity; and
- an observed increase in the coefficient of variation with an increase in wavelength, indicating that the coefficient of variation is frequency dependent.

By combining the quantified results from the above studies, the intra-method variability can be estimated. Figure 4.1 shows the mean or average V_{S30} measurement versus the coefficient of variation for a particular method. Based on these combined results, it is suggested that a reasonable estimate of intra-method variability for SASW is a $COV \approx 5\% - 6\%$. This includes different SASW sources, and varying processing and inversion techniques. MASW appears to have a similar coefficient of variation. ReMi appears to have a slightly lower coefficient of variation, but because the sample size is small here, and it is unclear if the lower observed coefficient of variation is an artifact of the test or from the paucity of data.

For invasive methods it is difficult to estimate the intra-method variability because it is a destructive test and repeating would require using the same borehole, which is not always feasible. The data shown on Figure 4.1 for the downhole measurements are based on the same downhole test with different post-processing of the data. Using different running averages of suspension log data can also result in slightly different V_{S30} measurements. It is anticipated that variability is present with the use of SCPT data as well. A rough estimate of the coefficient of variation for invasive tests is approximately 1–3%.

These suggested coefficients of variation may not be statistically significant because of the lack of data, yet represent all the published data that currently exist. These values do compare favorably to studies that have evaluated the coefficient of variation related to other tests that measure *in situ* properties of geologic material. Kulhawy and Mayne (1990) found that when measuring soil penetration resistance with the CPT (cone penetration test), the coefficient of variation due to epistemic uncertainty (equipment and procedure variability, not inherent randomness) was approximately 8%, which is similar to other *in situ* tests reported in the same reference. By presenting the existing data for V_{S30} variability, it is hoped that other researchers will be encouraged to perform repeated tests to increase the amount of data. Until that time the suggested coefficient of variation values appear reasonable enough for calculation purposes.

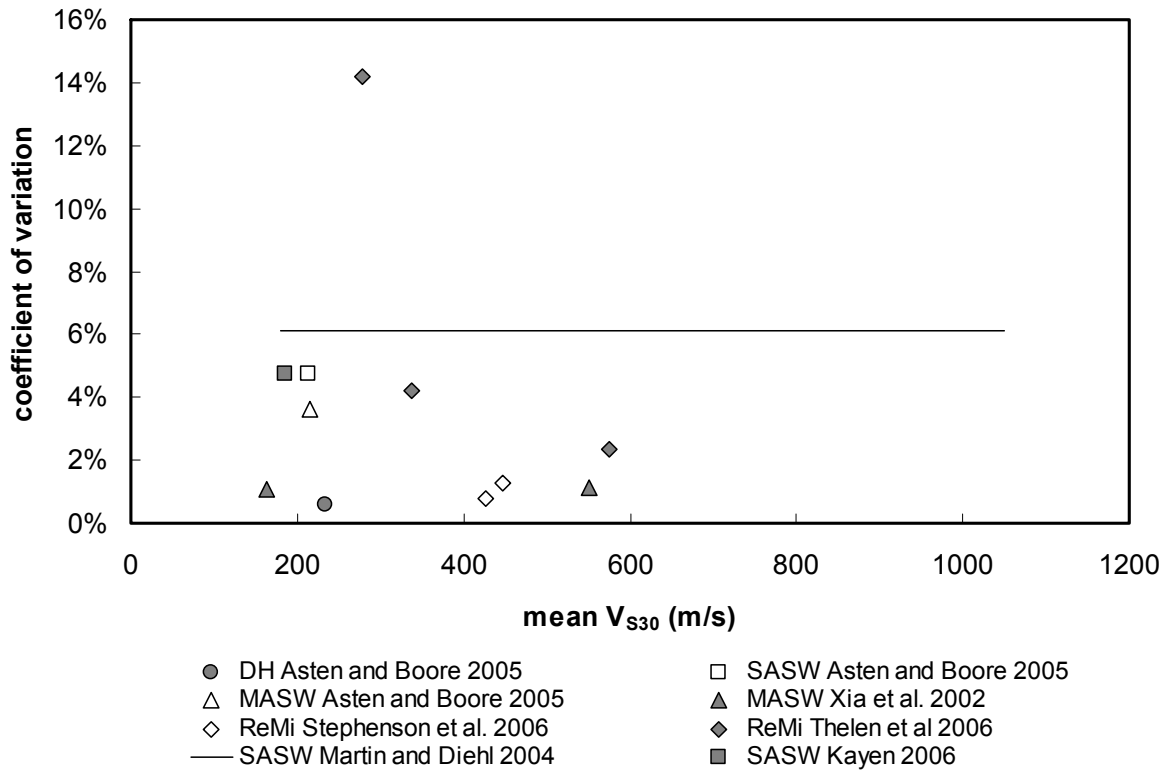


Fig. 4.1 Combined results from various studies showing intra-method variability.

4.1.2 Inter-Method Variability

The best means to assess the inter-method variability is to perform blind tests at as many sites as possible and evaluate the variations in the results. A deficit of the blind test is that there is no means of determining which test is providing a true mean; therefore the comparison is a relative measure of uncertainty with the potential for bias.

Generally, suspension logging measurements are thought to be the most accurate (Asten and Boore 2005) because the short, fixed distance between source to receiver means that the signal is always unambiguous (unless there are irregularities or breakouts in the borehole wall) and there is no increase in uncertainty with depth. Suspension logging, however, tends to be a small-scale measurement of the dynamic properties of the soil. Therefore it is common to use a running average of suspension logging data to represent the shear wave velocity of near-surface materials. Asten and Boore (2005) used a 5-point running average to smooth the suspension logging results, which results in 2.5 m resolution for 0.5 m sampling. Boore (2006) used an

average of all invasive methods for comparison with non-invasive methods. This approach is generally followed in this paper.

The suspension data acquired from various studies had sampling rates of 0.5 m or 1.0 m. To provide a consistent running average, a 3.0 m resolution was used here. For the 1.0 m sampling rate this required a 3-point running average. For the 0.5 m sampling rate this required a 6-point running average with two behind and three ahead of the current depth increment.

Two additional studies are cited here but not used in the analysis. The EPRI (1993) study of Gilroy2 and Treasure Island data was not available in tabular form and the hard copies of the Vs profiles were not clear enough for the data to be digitized; therefore this study was not included in the analysis. Liu et al. (2000) performed passive surface wave measurements at two sites where downhole measurements exist, but the upper 60 m were not evaluated using the surface wave method.

Table 4.2 List of blind studies used to quantify inter-method variability.

Blind Study	No. Sites	Methods Used
Louie (2001)	1	Suspension log, ReMi, Reflection
Brown et al. (2002)	10	Suspension log, SASW, Downhole
Xia et al. (2002)	4	Downhole, Suspension log, MASW
Rix et al. (2002)	4	SCPT, Reflect, Reflect/Refract, SW passive and active, VSP
Williams et al. (2003)	6	Downhole, Reflect/Refract
Martin and Diehl (2004)	54	SASW, ReMi, Suspension log
Asten and Boore (2005)	1	Downhole, SCPT, Suspension log, SASW, MASW, ReMi, SPAC, f-k, Reflect/Refract, HVSr
Stephenson et al. (2005)	4	Suspension log, SASW, ReMi

The studies in Table 4.2 used for inter-method uncertainty analysis are described briefly below:

- Louie (2001) presented ReMi measurements at 1 site where there was existing suspension logging data.

- Brown et al. (2002) evaluated the shear wave velocity (the inverse of slowness) at ten strong motions sites where downhole and/or suspension logging existed. The downhole and suspension logging were averaged to represent the invasive velocity measurement with which to compare the non-invasive (SASW) measurements.
- Xia et al. (2002) compared MASW measurements at four sites where there was downhole or suspension logging.
- Rix et al. (2002) investigated ten sites, but only four sites had a comparison of invasive versus non-invasive tests. The four sites included here compare surface wave measurements (using both passive and active sources) with SCPT measurements.
- Williams et al. (2003) compared reflection/refraction measurements at six sites with downhole measurements. They provided some preliminary statistical analysis of the comparison and a quick method for estimating V_{S30} based on first arrival time.
- Martin and Diehl (2004) evaluated SASW versus suspension logging at one site. The rest of the sites compare a simple SASW technique with SASW alone or SASW combined with ReMi measurements.
- Asten and Boore (2005) presented a blind study including nine different methods for measuring the shear wave velocity. This study evaluated only one site but was useful in providing multiple measurements using the same methods by different researchers.
- Stephenson et al. (2005) provided blind comparisons of ReMi, MASW, and suspension logging at four sites, of which two were viable for this study [(one had no shear wave velocity measurements above 50 m, and the second was included in Asten and Boore, (2005)].
- Jaume (2006) measured shear wave velocity at four sites using both SCPT and ReMi.

Figure 4.2 shows the results of all shear wave velocity methods presented in Asten and Boore (2005) with respect to suspension logging. SASW represents the largest statistical sample from this study, with results ranging 10% above and below the suspension logging results.

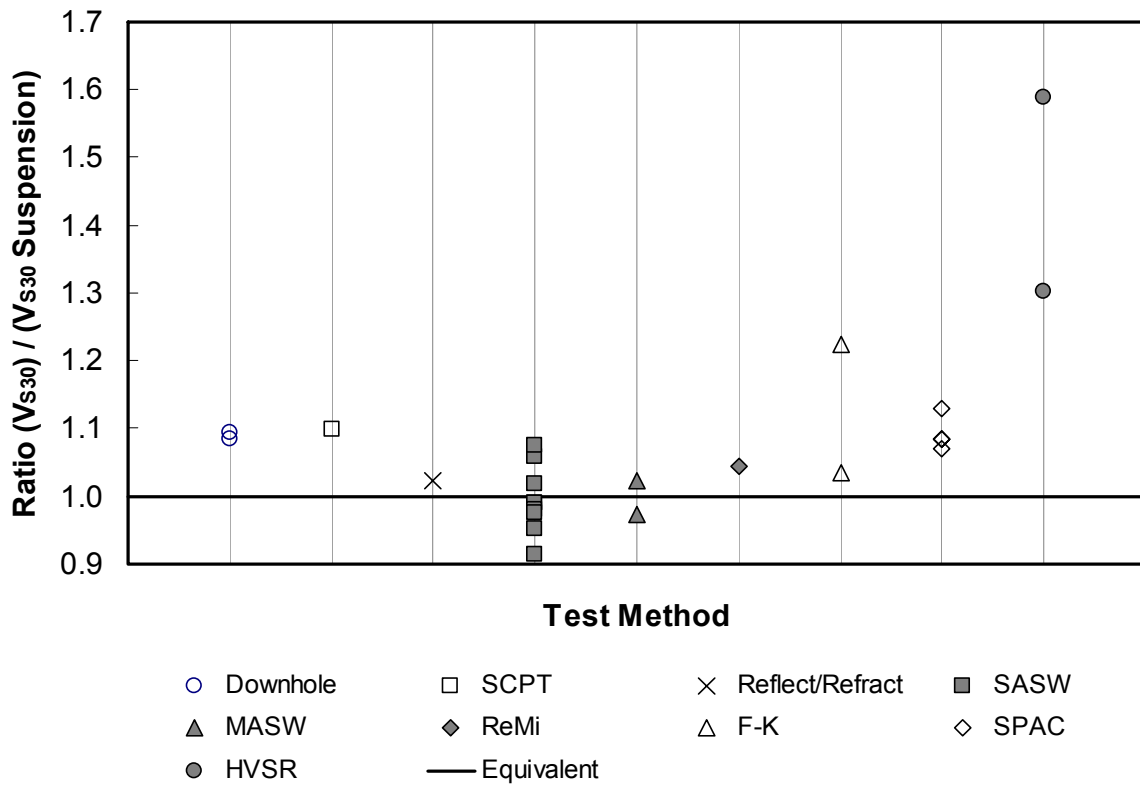


Fig. 4.2 Results from Asten and Boore (2005) showing nine V_{s30} test methods with respect to suspension logging.

A plot of blind study results, Figure 4.3, shows a bias between invasive methods (DH, suspension logging, and/or SCPT) and non-invasive methods (SASW, MASW, and SW). The data were plotted in this format because it provides an easy means of spotting trends or bias, similar to a residual plot of measured versus predicted values. No bias would appear as a random pattern around the 1.0 line; positive or negative bias would appear as a rising or falling trend in the data. The NEHRP C/D and B/C (BSSC 2001) site class boundaries are shown on Figure 4.3 for reference. For softer sites (lower shear wave velocities) non-invasive methods provide higher estimates than the invasive methods. For stiffer sites (higher shear wave velocities) non-invasive methods provide lower estimates than the invasive methods. This bias is similar but less prominent when evaluating reflection/refraction and ReMi methods (Fig. 4.4). It is important to note that for the reflection/refraction and ReMi there is a much smaller sample size than for SASW, MASW, and SW which may influence the trend.

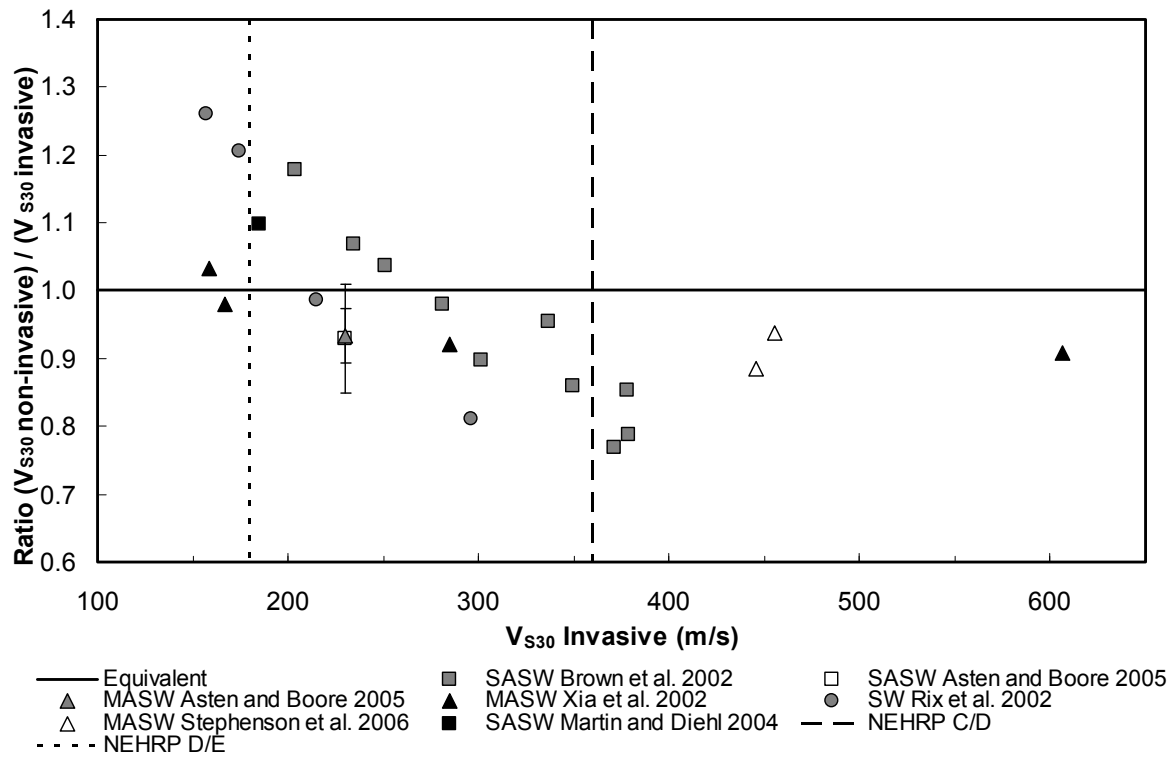


Fig. 4.3 Combined results of comparison studies showing inter-method variability for SASW and MASW.

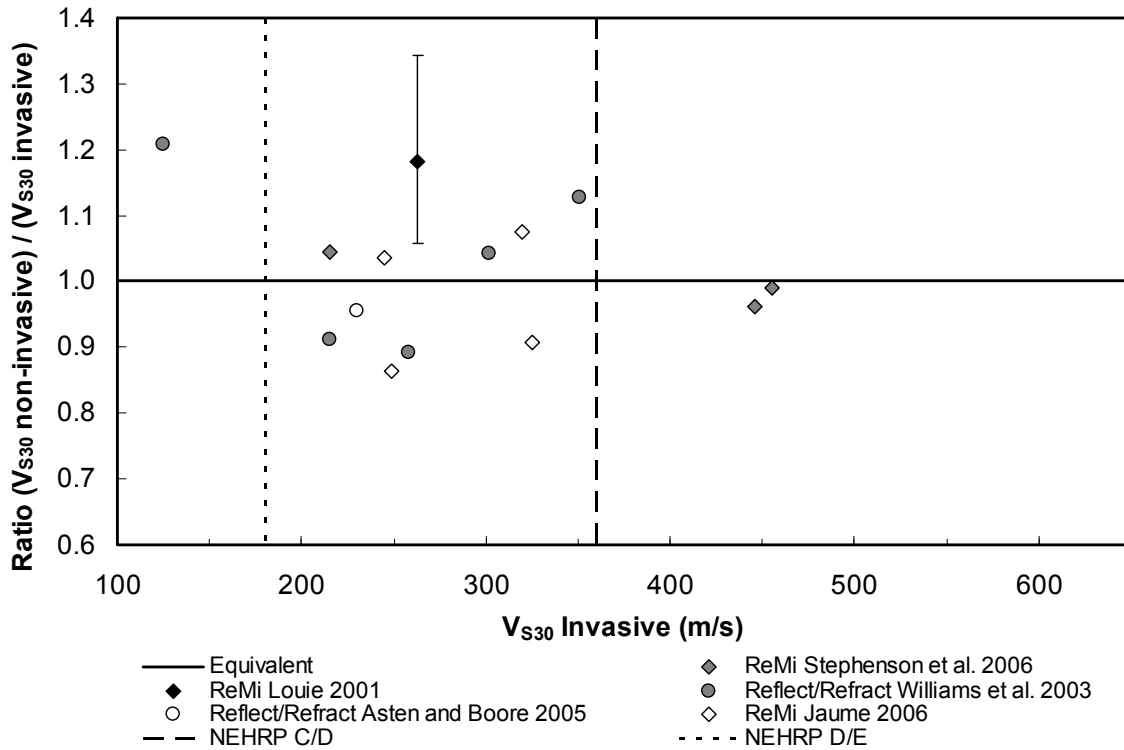


Fig. 4.4 Combined results of comparison studies showing inter-method variability for reflection/refraction and ReMi methods.

To evaluate the bias between invasive and non-invasive methods, two hypotheses of the cause of the bias were tested: (1) near-surface effects and (2) soil disturbance effects. The first hypothesis is that invasive methods tend to have difficulty measuring the upper few meters due to the lack of confinement. To test for this near-surface effect a subset of the data in Figure 4.3 was evaluated at a shear wave velocity interval from 5 m to 30 m (V_{S5-30}) to eliminate the impact of the upper 5 m. Figure 4.5 shows that based on this subset of data from Brown et al. (2002), near-surface effects are not likely contributing to the observed bias between invasive and non-invasive tests. The linear trends are roughly parallel, suggesting that no bias can be attributed to near-surface effects on invasive methods.

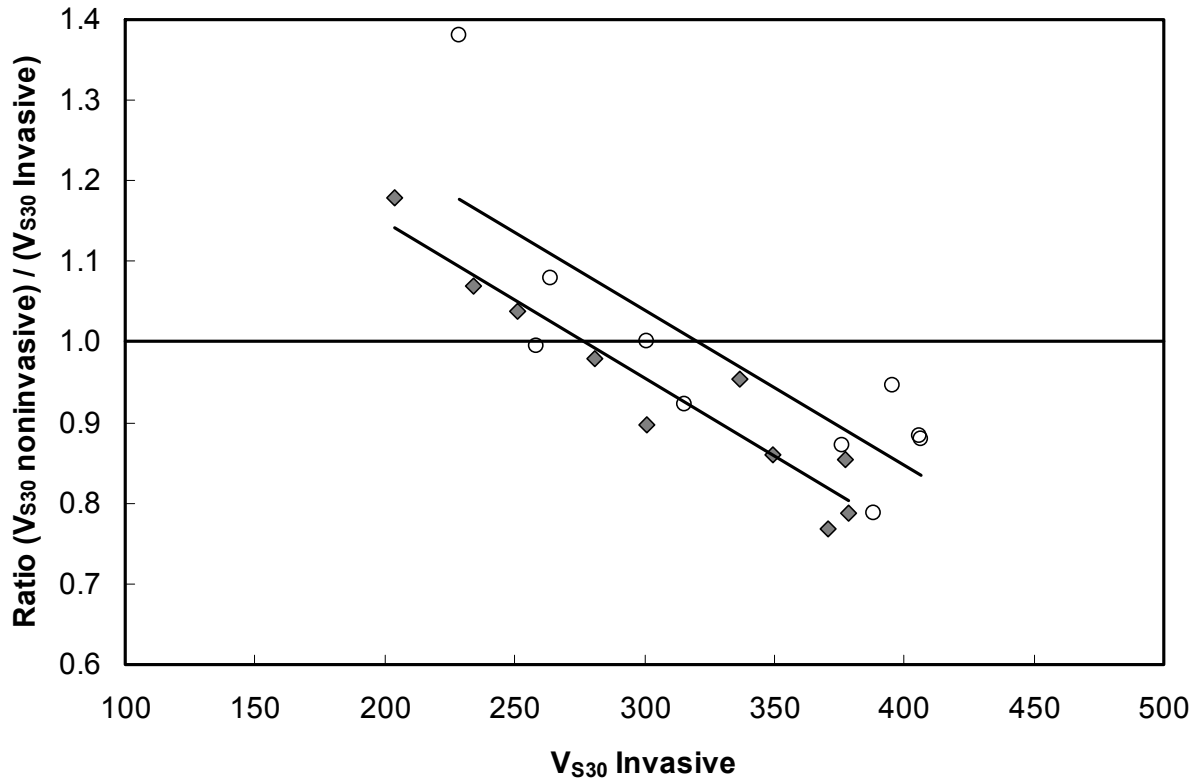


Fig. 4.5 Difference between V_{S30} and V_{S5-30} are shown to determine if near-surface effects are cause of bias between invasive and non-invasive methods. Diamonds are V_{S30} data and circles V_{S5-30} data, from sites presented in Brown et al. (2002). Linear trend lines show almost parallel slopes indicating no bias can be attributed to near-surface effects on invasive methods based on this hypothesis.

The second hypothesis, which can only be loosely examined with the limited data available, is that soil disturbance may influence invasive shear wave velocity measurements. It is conceivable that through the process of pushing a SCPT cone, or drilling a hole for the suspension logging or downhole measurements, the soil is disturbed enough to alter the shear wave velocity. For softer soils this could result in overall strain softening and in stiffer soils this could result in overall strain hardening, thereby producing the observed bias. Shear wave velocity is related to the soil stiffness or initial shear modulus (G_{max}) and the soil density (ρ) by the following equation:

$$V_s = \sqrt{G_{max} / \rho} \quad (4.1)$$

This soil disturbance effect should be most pronounced in suspension logging because small-scale shear wave velocity measurements are made directly around the device within close

proximity of the disturbed soil. The wave path for the suspension logging may be entirely through the zone of disturbed soil. For the SCPT and downhole the effect should be less pronounced because waves are traveling from a source at the surface and encounter disturbed soil only within the zone immediately around the receiver, thereby having minimal effect on the overall travel time.

Invasive methods can be considered analogous to pile driving and the results of how driven piles disturb the soil can provide insight into the modification of the soil stiffness with disturbance. Work by Hunt et al. (2002) evaluated the effect of pile driving on the dynamic soil properties in soft clay (average $V_{S30}=111$ m/s). It was found that strain softening occurred around the pile during driving, resulting initially in a reduction in shear wave velocity. The most immediate measurements were taken five days after pile driving, with results showing upwards of 25% decrease in shear wave velocity within 1 pile diameter from the face of the pile, and 5% or more decrease in shear wave velocity at distances greater than 3 pile diameters. These results showing an initial decrease in stiffness or shear wave velocity agree with lab testing in the same study and with work by previous researchers studying rate effects on the dynamic shear modulus of clays (e.g., Humphries and Wahls, 1968).

A study by Kalinski and Stokoe (2003) evaluated a new technique of borehole SASW testing for estimating *in situ* stresses. Great care was taken to minimize disturbance during the borehole excavation using incremental reaming, but the influence of soil disturbance on the shear wave velocity measurements was still observed. The soil conditions at the test site were stiff clay over silty sand, with testing conducted at a depth of 2.6 m in the silty sand. The results show a pronounced influence of soil disturbance on the shear wave velocity measurements within approximately 0.2 borehole diameters. The shear wave velocity within the disturbed zone was lower than in the “free field” soil, showing a 10–30% decrease from an average “free-field” shear wave velocity of approximately 200 m/s. The authors conjectured that shearing occurred in the medium-dense silty sand near the borehole wall and that dilation and an increase in void ratio was the likely cause of the decrease in shear wave velocity in the disturbed zone.

In general, laboratory testing of different soils subjected to low and high strains have found that the initial shear modulus (G_{max}) is a function of two variables that can be altered during disturbance, the mean effective stress and the void ratio (e.g., Hardin 1978; Jamiolkowski et al. 1991). An increase in void ratio will result in a decrease in initial shear modulus, whereas an increase in the mean effective stress will result in an increase in initial shear modulus. The

mean effective stress will change as a function of undrained soil behavior and pore pressure response. The void ratio will change as a function of drained soil behavior.

For clays, soil disturbance from invasive tests will result in undrained response because of the low permeability and the time it takes excess pore pressures to escape. For soft clays, as in Hunt et al. (2002), undrained soil behavior that results in positive excess pore pressure causes a decrease in the mean effective stress and a decrease in the initial shear modulus and shear wave velocity. The opposite would be true for stiff clays.

For sands the location of the water table will determine if undrained soil behavior is feasible, and the need for borehole casing will also impact the soil behavior. This makes for a complex response. During drilling, sand may initially respond in an undrained manner immediately adjacent to the new borehole wall. Installation of a casing will also result in some disturbance and can have uncertain results on the soil state. For suspension logging or downhole seismic enough time may have elapsed following the drilling and/or casing that the excess pore pressure will have dissipated and the soil resumes a drained state. In the case of pushing a cone, it has been found that most sandy soils will behave in a drained manner with respect to the standard push rate of 2 cm/sec (Lunne et al. 1997). Of interest is the cumulative effect and if it results in strain hardening or strain softening. Dense sandy soils will want to dilate and/or generate negative pore pressures when disturbed, and loose sandy soils will want to contract and/or produce positive pore pressures when disturbed. Whether shear wave velocity is measured when excess pore pressures are present or after the pore pressures have dissipated and the void ratio has changed will dictate if strain hardening or strain softening has occurred.

Although there are not sufficient data to statistically compare suspension logging with SCPT or downhole seismic, a qualitative comparison is made to support the soil disturbance hypothesis. Shown in Figure 4.6 are six sites where there was more than one invasive method used to measure V_{s30} . The data indicate that suspension logging tends to have higher shear wave velocity measurements for the stiffer sites and lower shear wave velocity measurements for the softer sites, when compared to other invasive measurements. This qualitative assessment and the other studies discussed above support the hypothesis that

- Soil disturbance has an influence on the measurement of shear wave velocity using invasive methods;
- Suspension logging is most influenced by soil disturbance because of its small-scale measurement of shear wave velocity; and

- Borehole excavation in softer soils can result in overall strain softening and a decreased shear wave velocity, and in stiffer soils soil can result in overall strain hardening and increased shear wave velocities.

Further research needed to confirm this hypothesis would include more blind studies with multiple invasive methods used at each site, as well as laboratory studies looking at the change in soil stiffness (and shear wave velocity) before and after shear failure.

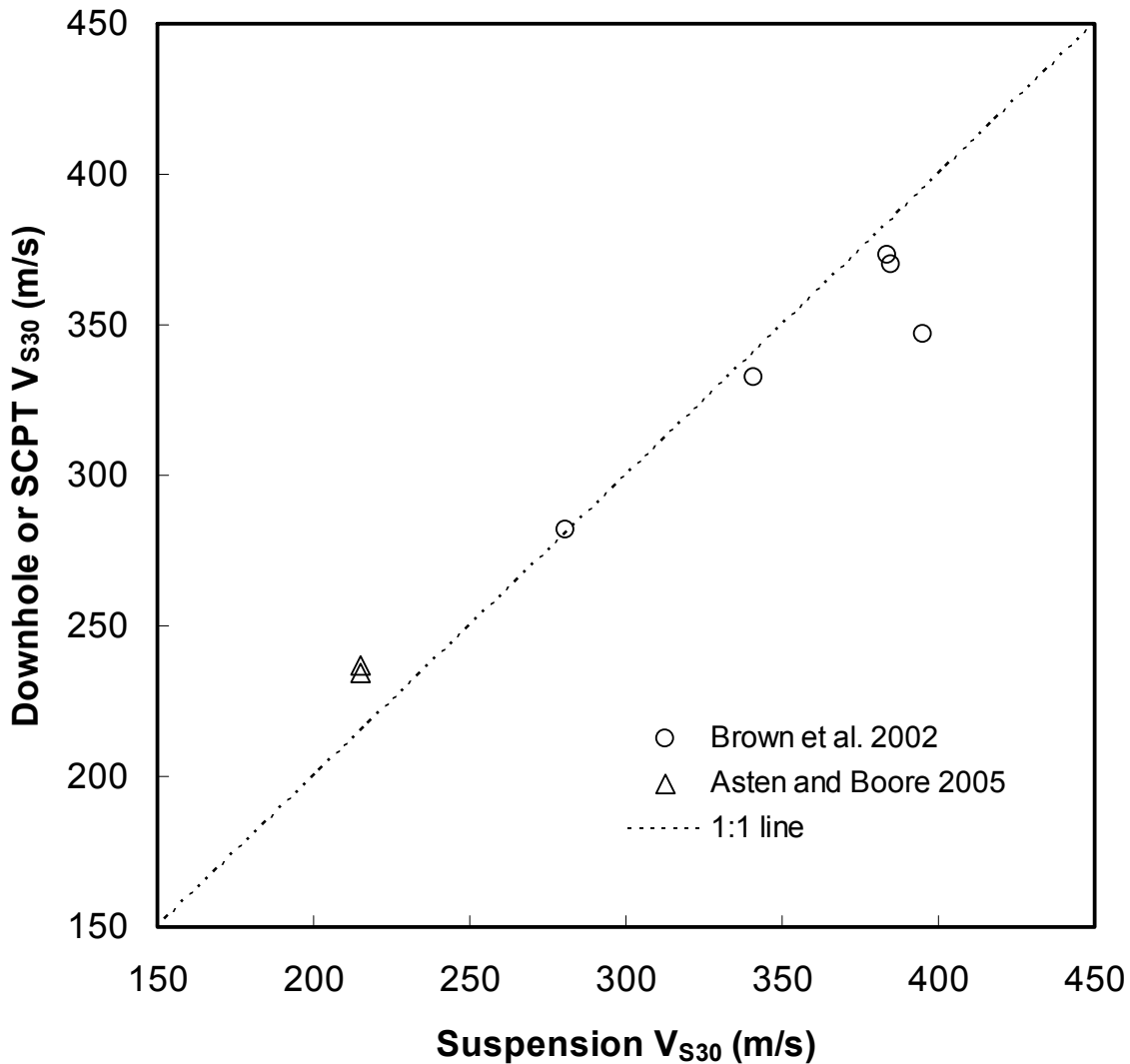


Fig. 4.6 Comparison of V_{s30} from suspension logging and downhole or SCPT at six sites. Brown et al. (2002) presented suspension logging and downhole data for each site. Asten and Boore (2005) presented one site with suspension logging, SCPT, and downhole seismic.

Based on the soil disturbance hypothesis and loose confirmation of this hypothesis, it is assumed that the V_{S30} bias is a product of invasive methods and will be treated as such. A linear regression is performed on the data in Figure 4.3 to arrive at a relationship between invasive and non-invasive methods. Figure 4.7 shows the linear regression trend line and the accompanying statistics of this linear fit. The linear fit indicates that for V_{S30} less than approximately 200 m/s, invasive measurements (suspension logging, downhole, and SCPT) will be biased low, and for V_{S30} greater than approximately 200 m/s, invasive methods will be biased high. Subsequent discussion provides guidance on how the bias should be treated in engineering calculations.

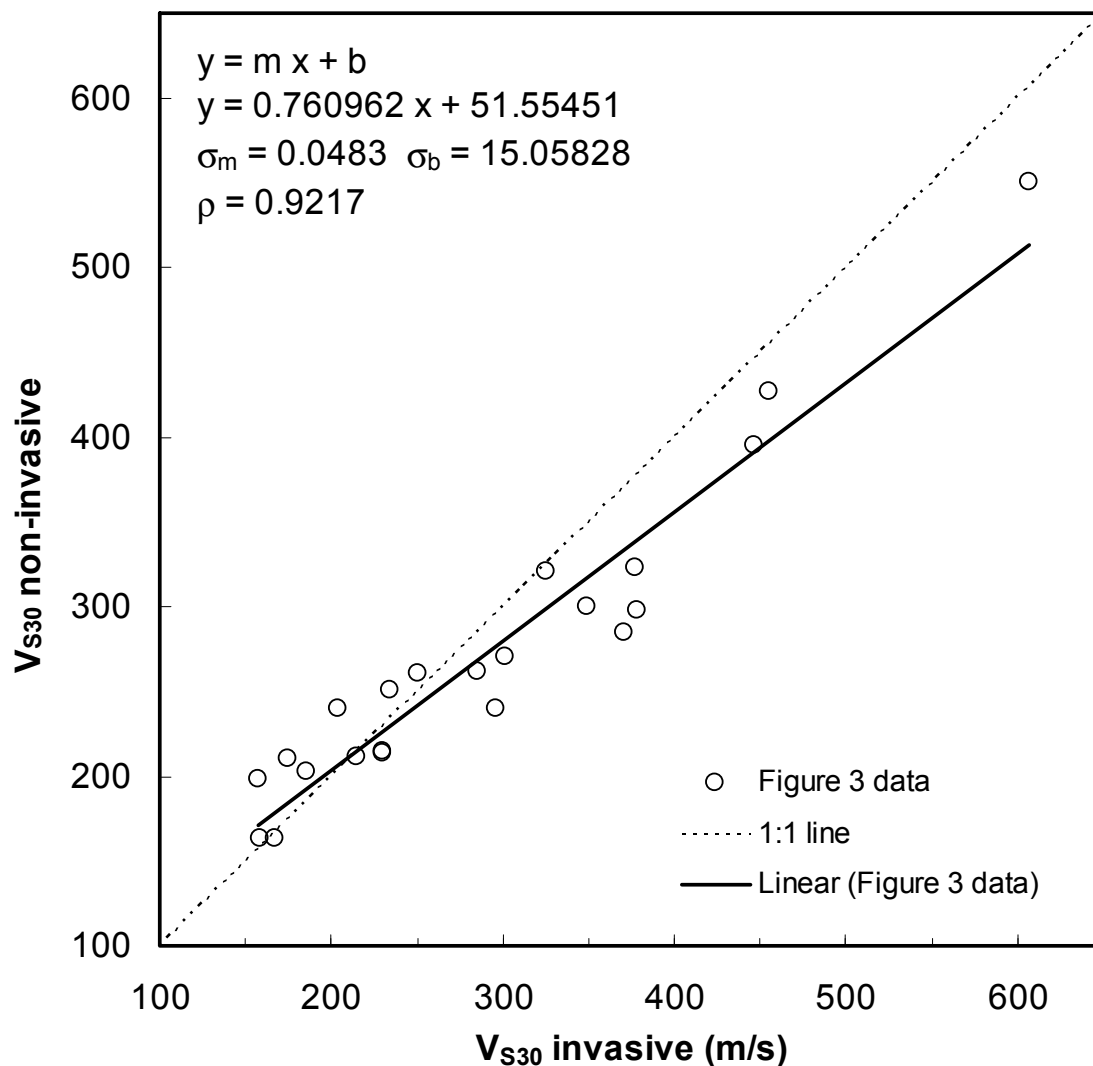


Fig. 4.7 Linear regression of invasive versus non-invasive; all data from Fig. 4.3. Statistics shown in upper left corner.

4.1.3 Variability of V_{S30} correlated Geologic Units

To provide a broader spatial coverage of V_{S30} estimates, Wills and Silva (1998) and Wills and Clahan (2004) studied the correlation of geologic units to V_{S30} measurements made within those units. Based on 19 generalized geologic units with sufficient V_{S30} measurements, Wills and Clahan (2004) presented the mean V_{S30} and standard deviation per unit. Estimating V_{S30} from surficial geology presents a case of combined measurement error, spatial variability, and model error. Figure 4.8 is the mean V_{S30} plotted against the coefficient of variation showing the measured uncertainty correlated to each geologic unit. The geologic unit names are shown next to each data point and the description of each geologic unit is presented in Table 4.3. A general trend of increasing coefficient of variation can be seen with increasing mean V_{S30} .

Table 4.3 Description of geologic units shown in Fig. 4.8 (after Wills and Clahan 2004).

Geologic Unit	Description
Qi	Intertidal Mud, including mud around the San Francisco Bay and similar mud in the Sacramento and San Joaquin delta and in Humboldt Bay
af/qi	Artificial fill over intertidal mud around San Francisco Bay
Qal, fine	Quaternary (Holocene) alluvium in areas where it is known to be predominantly fine
Qal, deep	Quaternary (Holocene) alluvium in areas where the alluvium (Holocene and Pleistocene) is more than 30m thick. Generally much more in deep basins
Qal, deep, Imperial Valley	Quaternary (Holocene) alluvium in the Imperial Valley, except sites in the northern Coachella Valley adjacent to the mountain front
Qal, deep, LA Basin	Quaternary (Holocene) alluvium in the Los Angeles basin, except sites adjacent to the mountain fronts
Qal, thin	Quaternary (Holocene) alluvium in narrow valleys, small basins, and adjacent to the edges of basins where the alluvium would be expected to be underlain by contrasting material within 30m
Qal, thin, west LA	Quaternary (Holocene) alluvium in part of west Los Angeles where the Holocene alluvium is known to be thin, and is underlain by Pleistocene alluvium
Qal, coarse	Quaternary (Holocene) alluvium near fronts of high, steep mountain ranges and in major channels where the alluvium is expected to be coarse
Qoa	Quaternary (Pleistocene) alluvium
Qs	Quaternary (Pleistocene) sand deposits, such as the Merritt Sand in the Oakland area
QT	Quaternary to Tertiary (Pleistocene-Pliocene) alluvium deposits such as the Saugus Fm of Southern CA, Paso Robles Fm of central coast ranges, and the Santa Clara Fm of the Bay Area
Tsh	Tertiary (mostly Miocene and Pliocene) shale and siltstone units such as the Repetto, Fernando Puente and Modelo Fms of the LA area
Tss	Tertiary (mostly Miocene, Oligocene, and Eocene) sandstone units such as the Topanga Fm in the LA area and the Butano sandstone in the SF Bay area
Tv	Tertiary volcanic units including the Conejo Volcanics in the Santa Monica Mtns and the Leona Rhyolite in the East Bay Hills
Kss	Cretaceous sandstone of the Great Valley Sequence in the Central Coast Ranges
serpentine	Serpentine, generally considered part of the Franciscan complex
KJf	Franciscan complex rock, including mélangé, sandstone, shale, chert, and greenstone
xtaline	Crystalline rocks, including Cretaceous granitic rocks, Jurassic metamorphic rocks, schist, and Precambrian gneiss

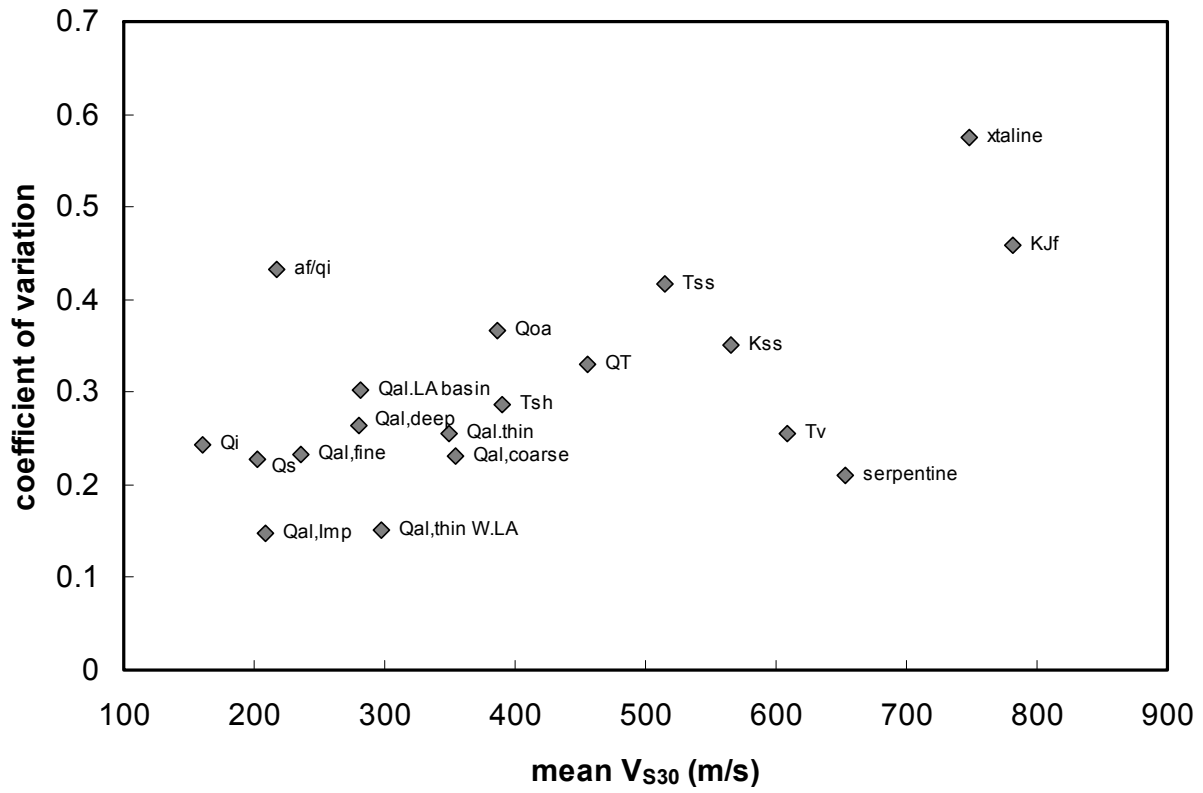


Fig. 4.8 Mean and coefficient of variation of V_{S30} for each of 19 generalized geologic units presented in Wills and Clahan (2004).

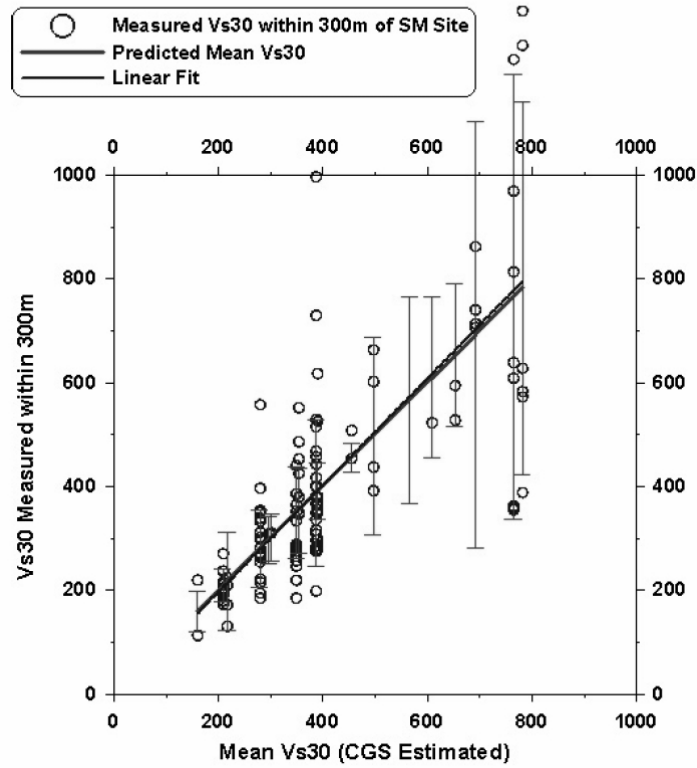


Fig. 4.9 Predicted versus measured V_{s30} from Wills and Clahan (2004).

Will and Clahan (2004) presented a comparison of the predicted V_{s30} at strong ground motion stations versus measurements made within 300 m of the station. Figure 4.9 shows a reasonably good fit between the predicted V_{s30} based on surficial geology and the V_{s30} measurements observed within the vicinity. The increase of variance with increasing shear wave velocity can also be observed in this plot.

To account for the increase in variance with an increase in shear wave velocity, a linear regression trend line is fit to the geologic unit correlated shear wave velocity data. The results in Figure 4.10 show a coefficient of variation of approximately 20–35%.

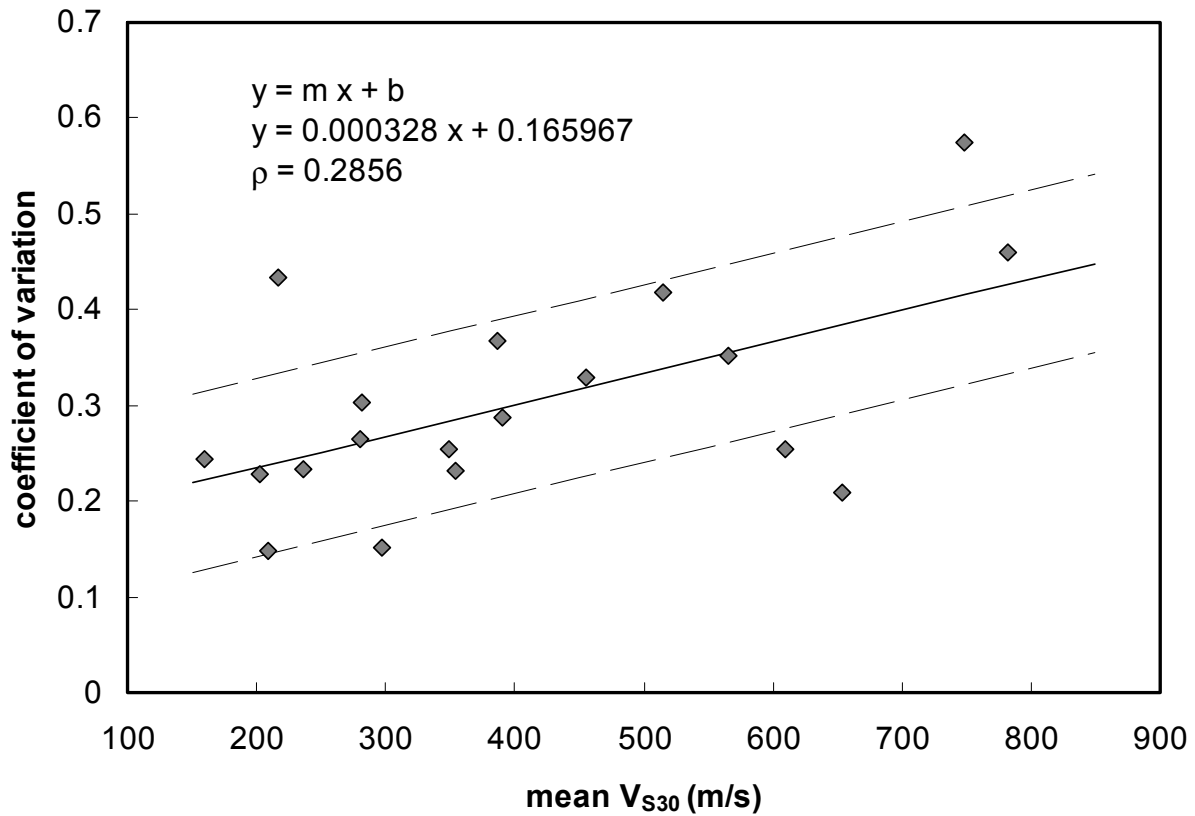


Fig. 4.10 Linear regression fit to trend of increasing coefficient of variation with increasing 30 m shear wave velocity for V_{S30} correlated geologic units. Mean and ± 1 standard deviation lines are shown. Regression results in the upper left corner.

4.1.4 Application of V_{S30} Uncertainty Point Estimate

Presented are estimates of apparent or observable measurement uncertainty based on existing comparative and blind studies. The focus is on 30 m shear wave velocity techniques used by the PEER Next Generation Attenuation (NGA) program. Based on the above analyses, this study finds the following:

- The intra-method coefficient of variation of the non-invasive method of SASW (and by similarity MASW) appears to be approximately 5–6% (Fig. 4.1).
- The intra-method coefficient of variation of invasive methods is difficult to quantify but is thought to be in the range of 1–3% (Fig. 4.2).
- The inter-method comparison of invasive versus non-invasive methods indicates a bias as a function of the V_{S30} value. This bias (Fig. 4.3) can be approximated with a linear trend line (Fig. 4.7), and is attributed to soil disturbance associated with invasive testing.

- The comparison between V_{S30} values and the correlated geologic units demonstrates an increasing coefficient of variation with increasing V_{S30} . This trend (Fig. 4.10) can be approximated with a linear fit.

The conclusions about the uncertainty in V_{S30} can be used in subsequent engineering calculations in the following manner.

If the shear wave velocity is based on **SASW**, a mean coefficient of variation of 5–6% is multiplied by the mean V_{S30} ($\mu_{V_{S30}}$) value to calculate the standard deviation estimate ($\sigma_{V_{S30}}$). Example: SASW measurements at a site produce a 30 m shear wave velocity of 250 m/s. The standard deviation is then 12.5–15.0 m/s ($\sigma_{V_{S30}} = (5 \text{ to } 6\%) \cdot \mu_{V_{S30}}$).

If the shear wave velocity is based on a **correlated geologic unit** the coefficient of variation is estimated using the mean linear trend line shown in Figure 4.10. This is multiplied by the mean V_{S30} ($\mu_{V_{S30}}$) value to calculate the standard deviation estimate ($\sigma_{V_{S30}}$). Example: A site is classified as Qal, deep, LA Basin, which correlates to a mean 30 shear wave velocity of 281 m/s; the standard deviation is then 72.5 m/s (from Fig. 4.10 the $c.o.v. = 0.000328 \cdot \mu_{V_{S30}} + 0.165967$ and $\sigma_{V_{S30}} = c.o.v. \cdot \mu_{V_{S30}}$).

If the shear wave velocity is based on an **invasive method (suspension logging, SCPT, and downhole)** then a coefficient of variation of 1–3% is multiplied by the mean V_{S30} value ($\mu_{V_{S30}}$) to calculate the standard deviation estimate ($\sigma_{V_{S30}}$). The mean from the invasive method can be adjusted for bias using the linear regression from Figure 4.7. The bias-corrected mean invasive shear wave velocity ($\mu'_{V_{S30}}$) is then

$$\begin{aligned}\mu'_{V_{S30}} &= (m \cdot \mu_{V_{S30}} + b) \\ \mu'_{V_{S30}} &= (0.760962 \cdot \mu_{V_{S30}} + 51.55451)\end{aligned}\tag{4.2}$$

Example: A suspension logging device measures the mean 30 m shear wave velocity at 300 m/s. The bias-adjusted mean calculated using Equation 2 is then 279.8 m/s. The standard deviation is then 2.8 m/s to 8.4 m/s ($\sigma_{V_{S30}} = (1 \text{ to } 3\%) \cdot \mu'_{V_{S30}}$).

These steps provide a best estimate of the uncertainty associated with V_{S30} measurements given the current state of knowledge and the existing blind and comparison studies available in the literature. These estimates will become more accurate in the future as more data are published on inter- and intra-method variability.

4.1.5 Spatial Variability of V_{S30} Measurements

Section 4.1 has thus far focused on the measurement uncertainty of V_{S30} , which is a point estimate of the bias and error in the measured site stiffness along a vertical column of geologic materials. When using correlated geologic units, spatial variability crept into these point estimates due to the nature of this method and the spatial distances over which averaged measurements were used for correlation. To better quantify spatial variability on a slightly more rigorous basis measured V_{S30} data were examined. There have been studies on spatial variability of soil properties, but Thompson et al. (2007) is the only study the author is aware of that looks at V_{S30} in particular, which is used here to quantify estimates of the spatial variability.

The semivariogram has been commonly used for mapping the spatial variability in geomaterials for purposes such as mining, geotechnical, and geo-environmental engineering (Isaaks and Srivastava 1989). The semivariogram is an effective means of visualizing and calculating the change in spatial variation with distance. Thompson et al. (2007) collected a database of SCPT and SASW V_{S30} measurements from the Bay Area and evaluated the spatial statistics (Fig. 4.11). They felt that there were not sufficient data to warrant fitting the SASW data with an exponential model and therefore published the results with a linear fit. However, as it was noted by the authors, a linear fit does not make logical sense when the distance approaches zero where we expect to see no variation as a function of distance.

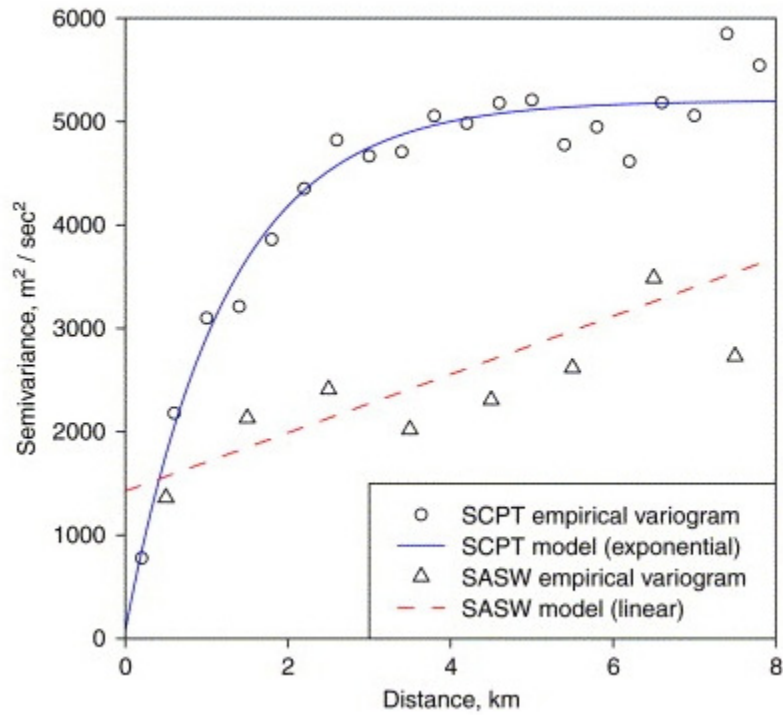


Fig. 4.11 Spatial variability of SCPT and SASW measured V_{s30} for an 8 km stretch in the Bay Area, from (Thompson et al. 2007) .

For approximation purposes, in this report the SASW was fit with an exponential model to provide an estimate of what an expected semivariogram would look like with sufficient data. Figure 4.12 shows this exponential fit which gives estimates of the semivariance for V_{s30} as measured using SASW. From this figure it can be seen that the spatial variation within 1500 m can be up to a standard deviation of 46 m/s (note: spatial standard deviation is the square root of semivariance).

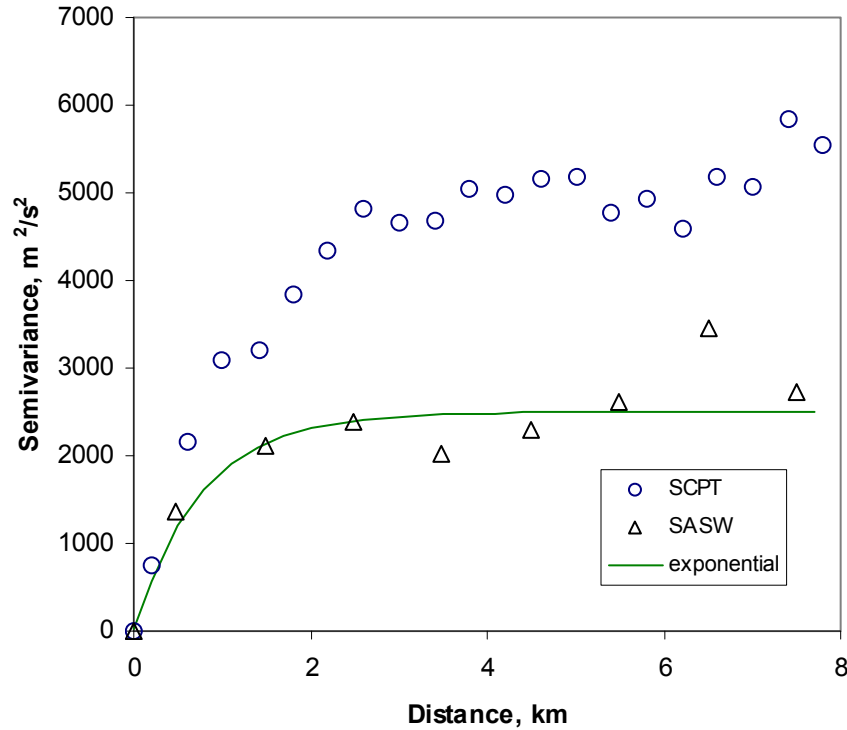


Fig. 4.12 Plot of Thompson et al. (2007) SASW data fit with exponential model.

4.1.6 V_{S30} Variance Results and Conclusions

Summarizing the above discussions of measurement uncertainty and spatial variability, the results can be generalized as

- For SASW and similar non-invasive V_{S30} measurement methods the $COV \approx 5\text{--}6\%$.
- For invasive methods $COV \approx 1\text{--}3\%$ and there exists a bias. A method of correcting for this bias was presented.
- For correlated geology methods the $COV \approx 20\text{--}40\%$. Geologic unit specific uncertainty has been presented based on previous work.
- An estimate of the spatial variability can be up to $\sigma \approx 46$ m/s (within 1500 m).

For the PEER NGA database the average V_{S30} uncertainty from measurement uncertainty, bias, and spatial variability for all recordings is approximately a $COV \leq 30\%$ using the information gathered in this study. This compares favorably to the estimated $COV \approx 27\%$ presented in (Chiou et al. 2008). As a confirmation of the quantified uncertainty, this study supports the work by Walt Silva as presented in Chiou et al. (2008) and achieves a consensus on

the general magnitude of measurement uncertainty and spatial variability present in the NGA database.

4.2 MOMENT MAGNITUDE (M_w)

The uncertainty of the moment magnitude can be attributed mainly to the inversion process used to calculate the seismic moment, and thus the moment magnitude. Moment magnitude is reported by seismology laboratories following an event, and iterated on for a week or two until the final revised value is reported. Calculating the moment magnitude involves an inverse problem to determine the seismic moment. The uncertainty in these calculations comes from the non-uniqueness of the inversion process.

Uncertainty in moment magnitude has also been shown to be a function of time. Kagan (2002) has estimated the standard deviation of the moment magnitude as a function of the inversion technique used to calculate the seismic moment. The accuracy and compatibility of different inversion techniques has improved over time, thereby providing a reduced standard deviation as we approach the present. Kagan reported a constant average standard deviation of $\sigma_{M_t}=0.081$ due to this time component for the moment tensor catalog that was analyzed.

The standard deviation of moment magnitude for any specific event (constant time) can be estimated from multiple reported magnitudes for each event where they exist. The standard deviation reported for the NGA database was based on the consideration of statistical standard deviation, time, and quality of the data and method used to derive magnitude (B. Chiou, personal communication, 2005).

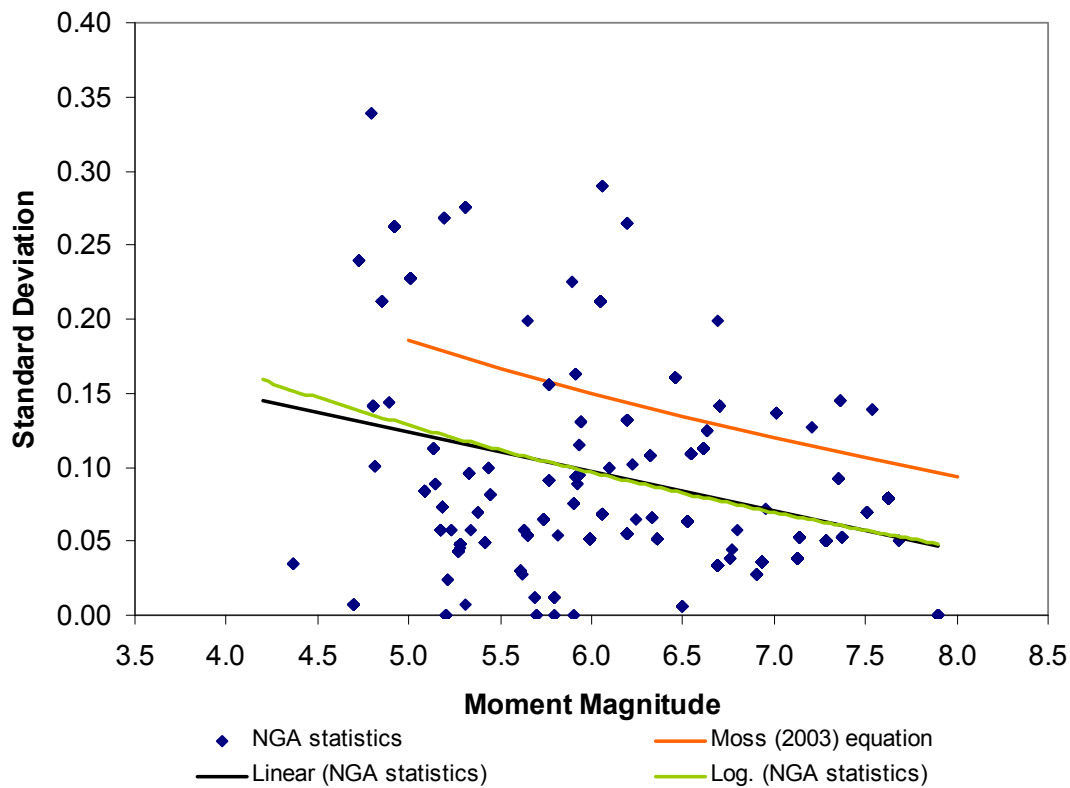


Fig. 4.13 Moment magnitude versus standard deviation of moment magnitude. Several lines have been fit to data, all showing a general decrease of variance with an increase in magnitude.

Figure 4.13 shows magnitude versus standard deviation as reported in the NGA dataset. There is a large amount of scatter in the data, but a general decrease in uncertainty with an increase in magnitude can be observed. This trend was conjectured by Moss (2003) based on the logic that for the inversion of seismic moment, the dimensions of the fault plane and the amount of slip associated with larger magnitude events tend to be easier to define than with smaller magnitude events. Uncertainty also stems from different inversion techniques used: partial or complete waveforms, regional or teleseismic recordings, and different Green's functions. (Caltech and Berkeley perform a regional inversion using complete waveforms; Harvard uses partial waveforms in a teleseismic inversion; and NEIC focuses on body waveforms in a teleseismic inversion.) Larger-magnitude events also have more stations recording the event (bigger sample size), generally have a higher signal to noise ratio, and have different seismology labs that may be using some of the same stations, resulting in correlated results.

Shown in Figure 4.13 are a linear regression line, logarithmic regression line, and the equation fit by Moss (2003). All three curves exhibit a similar slope, although the intercepts of the regression lines are lower. The Moss equation (2003) can be considered a high estimate corresponding to larger events, and the logarithmic regression line a reasonable mean estimate.

An attempt to elicit more refined results from the data was attempted, but both binning of the data and jackknifing produced ambiguous results. For forward or predictive analysis the regression with natural log function resulted in the following equation:

$$\sigma_{M_M} = -0.1820 \cdot \ln(M) + 0.4355 \quad (4.3)$$

The total measurement error associated with moment magnitude is then the sum of the variances:

$$\sigma_M^2 = \sigma_{M_t}^2 + \sigma_{M_M}^2 \quad (4.4)$$

More work needs to be done in quantify the uncertainty from moment magnitude.

The above equations can be used to make rough estimates, but some careful studies would be useful in determining the source of the uncertainty. The final results in this report (i.e., how measurement uncertainty influences ground motion prediction equations) do not include the quantified impact of measurement uncertainty from moment magnitude; that will be left for future studies.

4.3 DISTANCE (R)

Attenuation of seismic waves is controlled in a large part by the geometric spreading away from the earthquake hypocenter (centroid of energy release), thereby decreasing the energy per unit volume. After an earthquake occurs, the hypocenter is determined by triangulating from multiple recordings to find the coincident point of energy release. Refinement of the hypocentral location is part of the same inversion process used to determine the moment magnitude. This means that moment magnitude and distance are correlated. Some factors that result in uncertainty of the site-to-source distance measurement:

- The acceptable tolerance for resolving the hypocentral distance in the inversion process.
- Different rupture geometries (e.g., strike-slip versus dip-slip) that can affect the accuracy of the measurement of the hypocenter.

- Multiple or complex ruptures make determining a hypocenter for the event ambiguous. For example, the 2002 Denali, Alaska, earthquake had three subevents that produced the observed strong ground shaking (Harp et al. 2003).
- Several different metrics are used to measure distance within the strong ground motion attenuation modeling community. The most common distance metrics are R_{jb} , the closest horizontal distance to the vertical projection of the rupture, R_{rup} the closest distance to the rupture surface, R_{seis} the closest distance to the seismogenic rupture surface, R_{epi} the closest distance to the epicenter, and R_{hypo} the hypocentral distance (Abrahamson and Shedlock 1997).
- There is no consensus about the most appropriate metric for measuring distance, which indicates some uncertainty as to which distance measure is more accurate or most representative.
- There could be uncertainty introduced into the distance measure as a function of differing coordinate systems. The hypocenter may be located using WGS84 but the distance measure may be made in some other coordinate system, resulting in a loss of accuracy.
- In forward analysis where a ground motion prediction equation is used to predict future strong ground shaking, depending on the size of the site in question there may be some uncertainty as to the start of the distance measure. This can be a problem for big sites and small site-to-source distances. An example of this would be a project like the Oakland-San Francisco Bay Bridge where the site extends for several kilometers. This can be dealt with by estimating ground motion for multiple site locations, or using incoherency or transfer functions to propagate and attenuate motions along the site. But the exact start of the distance measure can present some uncertainty.

Discussions with UC Berkeley seismologists Doug Dreger and Bob Uhrhammer (personal communication, May 2007) provided some useful insight into the uncertainty of site-to-source distance. The precision of the location estimate is a function of station density. Precision can be approximately 200 m in epicentral location and 300 m in depth with high proximal station density, and 10–20 times that with low proximal station density. The accuracy of the hypocentral distance is influenced by the tolerance used for performing the inversion. For high proximal station density the acceptable location tolerance can be approximately 500 m, for low proximal station density, as much as 10 times higher. Differing coordinates systems can have an influence on the order of hundreds of meters. In California the difference between

NAD27 and WS84 is approximately hundreds of meters in longitude and tens of meters in elevation. This difference can be greater in other parts of the U.S. Uncertainty can also arise when determining distances geographically rather than geocentrically. This information has been summarized in the table below.

Table 4.4 Summary of contributors to distance uncertainty.

<u>Inversion Precision</u>	
-High station density	~200 m horizontal, 300 vertical
-Low station density	~10 to 20 times the precision above
<u>Inversion Tolerance</u>	
-High station density	~500 m
-Low station density	~10 times the tolerance above
<u>Coordinates System Error</u>	
(WGS84 vs. other)	~100's m in longitude and 10's m in elevation

These fixed uncertainties are a function of recording station density and the coordinate system, and in total are approximately 1–10 km in epicentral distance and 1–12 km in depth. The “three sigma rule” (Dai and Wang 1992) can be used to estimate the standard deviation based on the fixed uncertainties. The uncertainties are added and subtracted from the distance estimate to get the highest and lowest potential values, the difference of which is then divided by six. This assumes that the highest and lowest potential values define 99.73% of all possible values as measured by three sigma on either side of the mean of a normally distributed random variable:

$$\sigma_R = \frac{(R^+) - (R^-)}{6} \quad (4.5)$$

where R^+ and R^- are the distance estimates \pm the fixed uncertainties. This uncertainty is present in the ground motion database and contributes to the overall uncertainty in ground motion prediction equations. This fixed uncertainty will obviously have a dramatic impact on short distances or close in events, particularly for events that are poorly instrumented.

A form of uncertainty that comes into play in forward modeling or in the use of ground motion prediction equations for seismic hazard estimates is due to different distance metrics. This uncertainty would have an impact when performing a seismic hazard analysis where multiple ground motion prediction equations are used in a logic tree. As discussed, there are five common distance measures: R_{jb} the closest horizontal distance to the vertical projection of the rupture, R_{rup} the closest distance to the rupture surface, R_{seis} the closest distance to the seismogenic rupture surface, R_{epi} the closest distance to the epicenter, and R_{hypo} the hypocentral distance. Scherbaum et al. (2004) studied the relationship of these distance metrics and ran simulations to assess the relative variability. R_{jb} was treated as the baseline distance metric and the variation of R_{rup} , R_{seis} , R_{epi} , and R_{hypo} were calculated using simulated ruptures along a rupture plane scaled to magnitude. There is no justification to use R_{jb} over the other distance metrics, other than one metric needed to be fixed for comparison. The resulting frequency distributions of the variability of distance with respect to R_{jb} were best fit using a gamma distribution. For lower magnitudes the gamma distributions were approximately lognormal in shape, becoming more skewed and approximately exponential in shape at higher magnitudes. Figure 4.14 shows the coefficient of variation of each distance metric with respect to R_{jb} for different magnitudes over the distance bin of 5–15 km, the near-fault range where metric differences are the largest. The coefficient of variation can be rather high for larger-magnitude events, generally in the range of 50%–100%. The nominal or mean coefficient of variation for all results is shown in Figure 4.15. This figure better represents the contribution from differing distance metrics because no one method is considered fixed and the general contribution of uncertainty in a probabilistic logic tree can be estimated from these averaged results. For close-in distances (5–15 km) the variation between distance metrics can be large, with standard deviations on the same order as the mean values. This can have a dramatic impact on the resulting spectral acceleration values from different prediction equations. By including the uncertainty between distance metrics, the contribution of this form of epistemic uncertainty can be quantified and appropriately accounted for.

It is apparent from these figures that distance uncertainty with respect to distance metrics is strongly correlated with magnitude. This is also the case with the fixed uncertainties of distance uncertainty. At this stage more research needs to be conducted to better refine and quantify uncertainty from distance and how the correlation between distance and magnitude propagate through the ground motion prediction equation. From the preliminary analysis

included in this report the fixed measurement uncertainties can be large for near-fault distances with coefficient of variations in the 50%–100% range. For forward modeling with multiple prediction equations, the variability between distance metrics can be on the same order. The final results in this report (i.e., how measurement uncertainty influences ground motion prediction equations) do not include the quantified impact of measurement uncertainty from distance, which will be left for future studies.

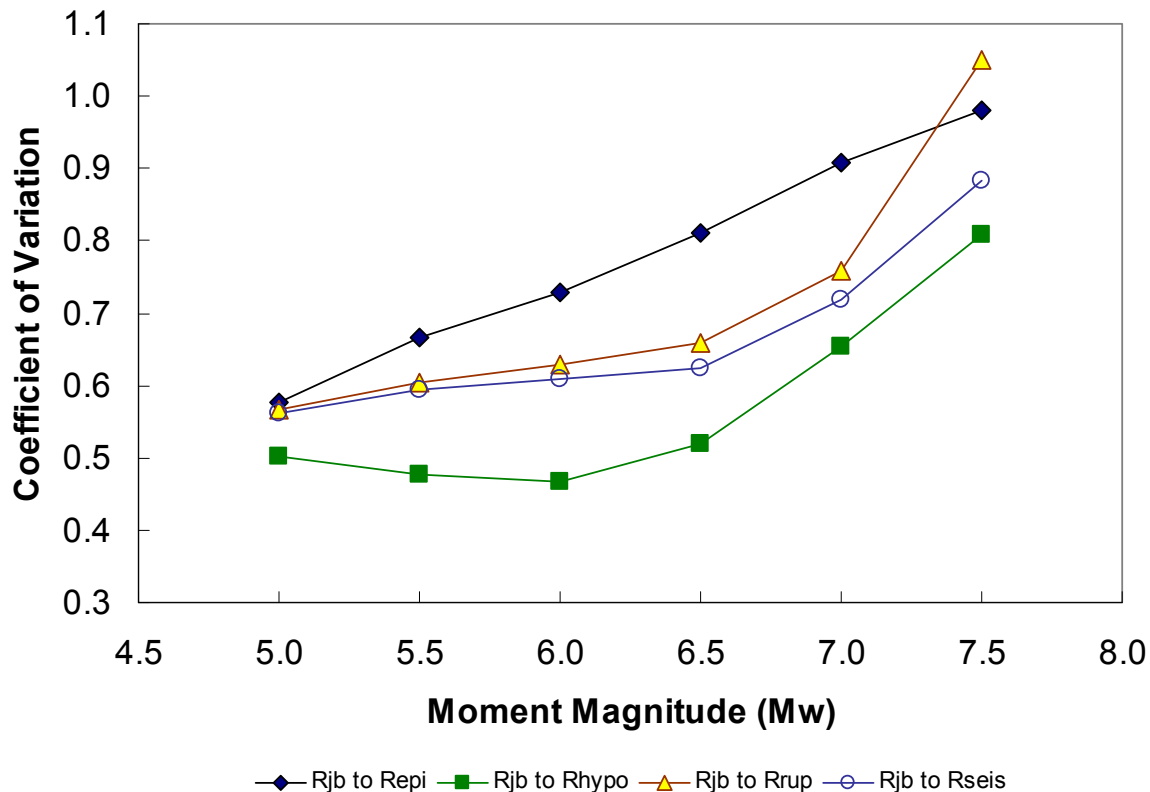


Fig. 4.14 Coefficient of variation of each distance metric with respect to Joyner-Boore, R_{jb} , distance for different magnitudes, and distance bin of 5–15 km (after Scherbaum et al. 2004).

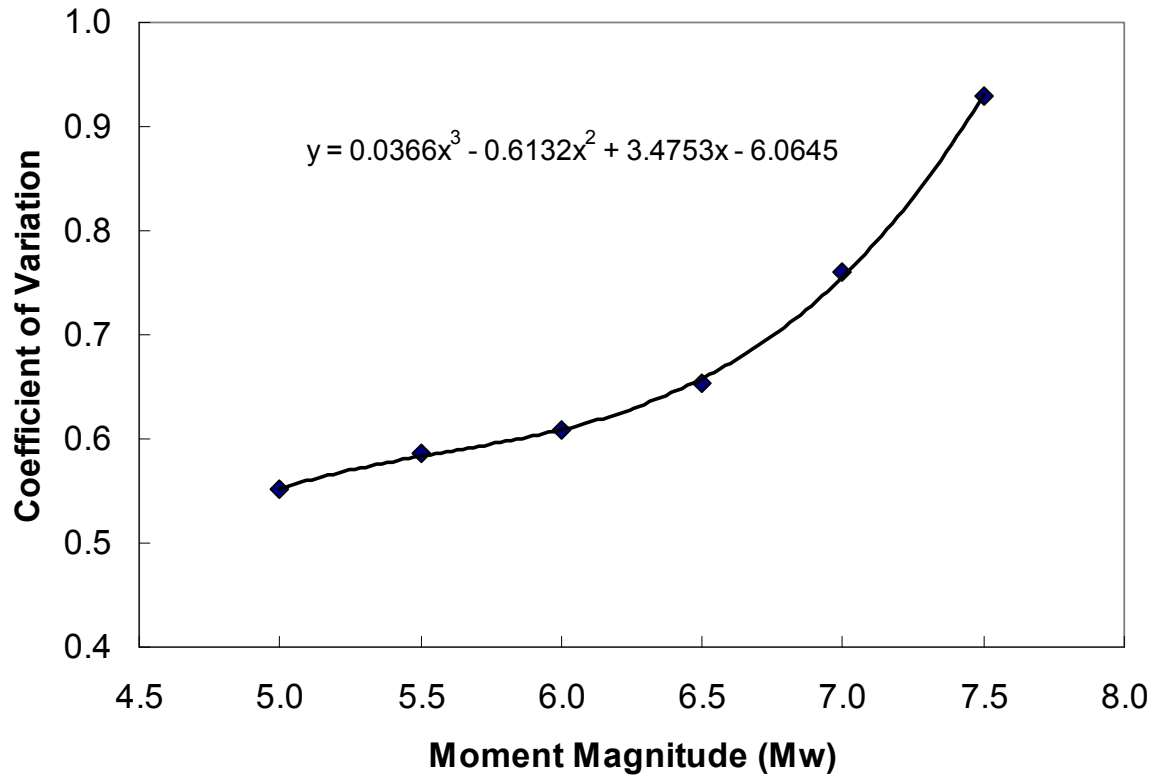


Fig. 4.15 Nominal or mean trend of the coefficient of variation of distance for various distance metrics, magnitudes, and distance bin of 5–15 km, with a polynomial fit for estimation purposes.

5 Implementation and Results

The culminating results of this study show the influence of V_{S30} measurement uncertainty on a ground motion prediction equation. This differs from the feasibility study in that a NGA ground motion prediction equation is used as the limit state, and quantified V_{S30} measurement uncertainty is applied to the NGA database. Bayesian regression was used to fit the (Chiou and Youngs 2008) model to the NGA database while accounting for the specific measurement uncertainty from the NGA database strong motion recordings. The Bayesian regression results are compared to and corroborated by two approximate solutions using first-order second-moment (FOSM) and Monte Carlo simulation (MC) techniques. These approximate solutions have the added benefit that they can be used for quick estimates when using other ground motion prediction equations as the basis, rather than resorting to a full Bayesian regression. Finally the Boore et al. (1997) prediction equation from the feasibility study is readdressed using the quantified V_{S30} measurement uncertainty, providing a comparative analysis with a simpler limit-state function.

5.1 CHIOU AND YOUNGS ATTENUATION MODEL

The driving focus of this study was to implement the Bayesian regression procedures with an NGA model. The Chiou and Youngs (2008) model was chosen because at the time of this research it was sufficiently complete and readily available. The ground motion prediction equation developed by Chiou and Youngs (2008) is defined by the following equations:

$$\begin{aligned}
\ln(SA_{1130ij}) = & c_1 + (c_{1a}F_{RVi} + c_{1b}F_{NMi})(1 - AS) + c_{10}AS + (c_7(1 - AS) + c_{7a}AS)(Z_{TORi} - 4) \\
& + c_2(\mathbf{M}_i - 6) + \frac{c_2 - c_3}{c_n} \ln(1 + e^{c_n(c_M - \mathbf{M}_i)}) \\
& + c_4 \ln(R_{RUPij} + c_5 \cosh(c_6(\mathbf{M}_i - c_{HM}, 0)_{\max})) \\
& + (c_{4a} - c_4) \ln\left(\sqrt{R_{RUPij}^2 + c_{RB}^2}\right) \\
& + \left\{ c_{\gamma 1} + \frac{c_{\gamma 2}}{\cosh((\mathbf{M}_i - c_{\gamma 3}, 0)_{\max})} \right\} \cdot R_{RUPij} \\
& + c_9 \cdot \cos^2 \delta_i \cdot \tanh\left(\frac{R_{RUPij}}{2}\right) \tan^{-1}\left(\frac{W_i \cos \delta_i}{2(Z_{TORi} + 1)}\right) \frac{1}{\pi/2} \left\{ 1 - \frac{R_{JBij}}{R_{RUPij} + 0.001} \right\} \\
& + \tau \cdot z_i
\end{aligned} \tag{5.1}$$

where the V_{S30} dependent function is defined by

$$\begin{aligned}
\ln(SA_y) = & \ln(SA_{1130ij}) + \phi_1 \cdot \left(\ln\left(\frac{V_{S30ij}}{1130}\right), 0 \right)_{\min} \\
& + \phi_2 \cdot \left\{ e^{\phi_3((V_{S30}, 1130)_{\min} - 360)} - e^{\phi_3(1130 - 760)} \right\} \cdot \ln\left\{ \frac{SA_{1130ij} + \phi_4}{\phi_4} \right\} + \sigma \cdot z_{ij}
\end{aligned} \tag{5.2}$$

and the terms of the equations are

- $\ln(SA_y)$ = natural log of spectral acceleration
- $\ln(SA_{1130})$ = natural log of spectral acceleration of "rock"
- R_{rup} = closest distance to rupture plane (km)
- R_{jb} = Joyner - Boore distance to the rupture plane (km)
- δ = rupture dip
- W = rupture width (km)
- Z_{TOR} = depth to top of rupture (km)
- $F_{RV} = 1$ for $30^\circ \leq \lambda \leq 150^\circ$, 0 otherwise
- $F_{NM} = 1$ for $-120^\circ \leq \lambda \leq -60^\circ$, 0 otherwise
- λ = rake angle
- V_{S30} = average shear wave velocity for the upper 30 m (m/s)
- τ = inter - event standard error
- σ = intra - event standard error

Bayesian regression was used to mimic the Chiou and Youngs (2008) results using exact parameters in what the authors termed step 1 regression of the first phase of the analysis; a regression of the NGA database neglecting hanging/footwall effects and soil nonlinearity effects. Description of which data from the NGA database were selected for regression can be found in detail in Chiou and Youngs (2008). The Bayesian regression mimicked the “classic” regression well as can be seen by the fit of the site-dependent function in Figure 5.1.

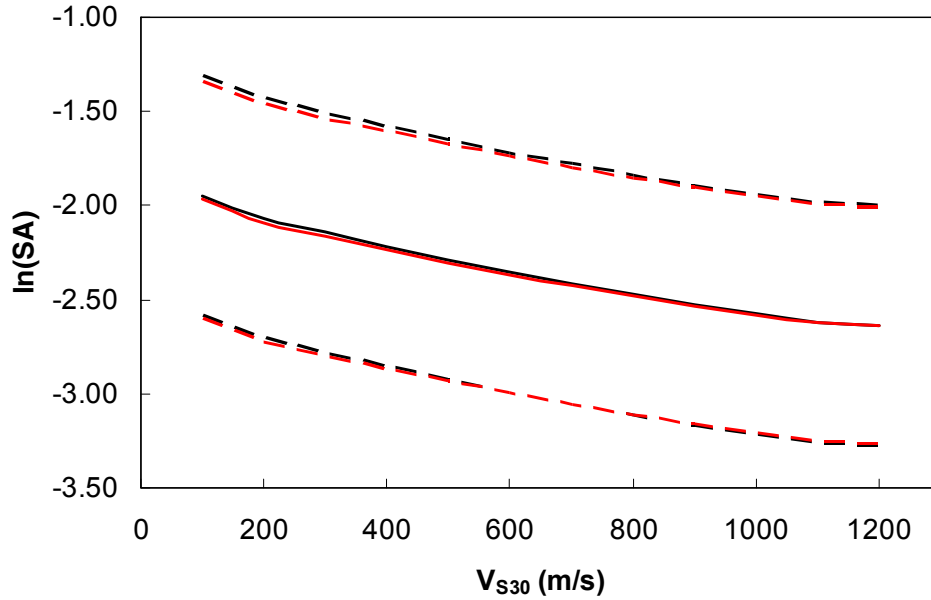


Fig. 5.1 Plot of V_{S30} versus natural log of spectral acceleration showing Bayesian regression duplicating “classic” regression with Chiou and Youngs (2008) model as limit-state function for period of 0.01 sec (PGA).

For the variance analysis the terms $\phi_1, \phi_2, \phi_3, \phi_4$, and σ are treated as random variables with parameter uncertainty, the ϕ terms being regression coefficients, and the σ term being the site-dependent or intra-event standard deviation in natural log units. The measurement uncertainty for each ground motion recording station according to the specific measurement method was taken into account with an overall database average of $COV \approx 27\%$. Bayesian regression was run for the spectral periods of 0.01 (PGA), 0.1, 0.3, 1.0, 3.0, and 7.5 sec. The percent decrease in the standard deviation of the $\ln(SA)$ is plotted in Figure 5.2. The decrease is shown with error bars because the Bayesian regression procedure is iterative, using a numerical solution that resolves the answer within a prescribed tolerance as specified by a coefficient of variation on the mean results ($COV \leq 25\%$ is considered a reasonable convergence). It can be

seen that the average decrease of the site-dependent error term is below 4% in the short periods and up to 9% at longer periods. These results are specific to the model formulation and how the inexact parameter, here V_{S30} , is treated in the model. The period dependent results indicate that V_{S30} influences the correlation more in the longer periods, with the most influence occurring at the 3 sec period. Figure 5.3 shows the 3.0 sec period comparison of Chiou and Youngs (2008) versus Bayesian regression results.

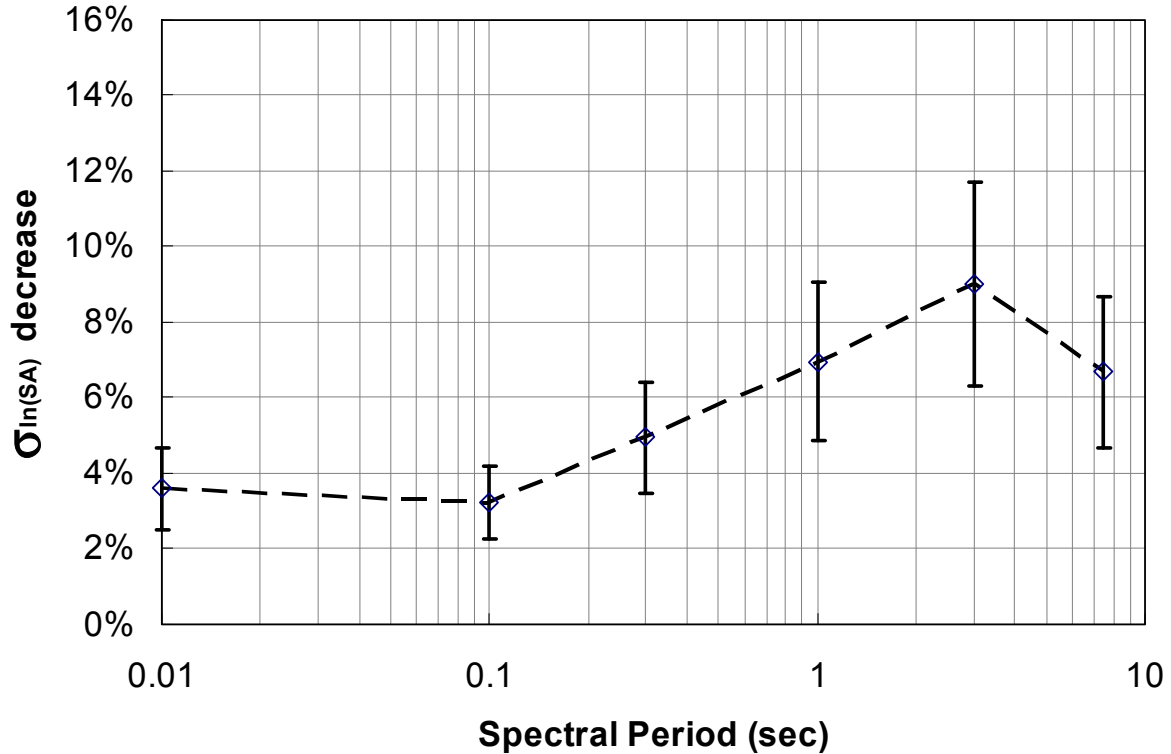


Fig. 5.2 Percent decrease in standard deviation of $\ln(SA)$ for different spectral periods. Database average V_{S30} measurement uncertainty taken into account was $COV \approx 27\%$. Error bars show convergence tolerance as a standard deviation of results for each spectral period.

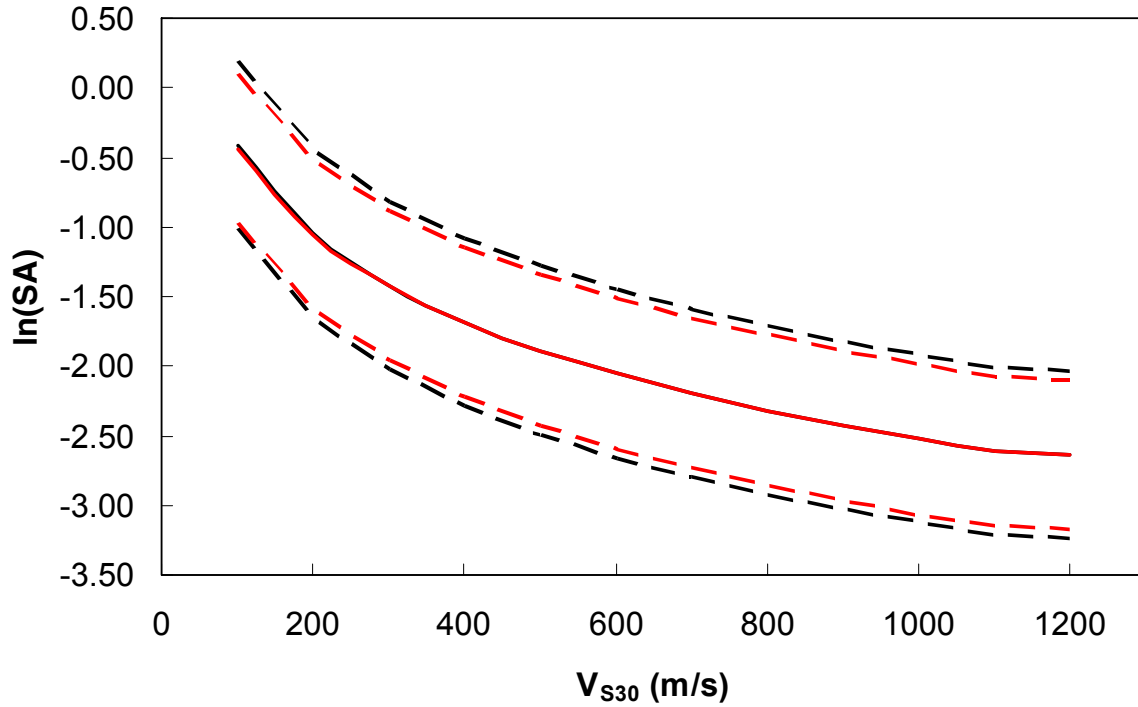


Fig. 5.3 Plot showing 3.0 sec period results. Decrease of 9% in standard deviation of $\ln(SA)$ is realized by taking into account V_{S30} measurement uncertainty using Bayesian regression.

5.2 APPROXIMATE SOLUTIONS

The Bayesian regression results are promising for reducing the model variance by accounting for parameter uncertainty but the procedure can be rather cumbersome. To provide confidence in the Bayesian regression results and provide a simplified method of performing variance analysis, two approximate solutions were evaluated; first-order second-moment (FOSM) and Monte Carlo simulations (MC).

5.2.1 First-Order Second-Moment Method

The first-order second-moment (FOSM) method is a basic approach to propagating uncertainty through a function. In this case we are propagating the uncertainty from input parameters through the ground motion prediction equation to determine how much the parameter uncertainty contributes to the overall uncertainty of the prediction. This method tends to be insensitive to nonlinear functional behavior and is evaluated only at the mean points. A Taylor series

approximation truncated after the first two terms is used to calculate the partial derivative of the ground motion equation with respect to the parameter of interest. For the case of Chiou and Youngs (2008), the FOSM analysis requires partial derivative of the site-dependent function (Eq. 5.2) with respect to V_{S30} :

$$\frac{\partial \ln(SA)}{\partial V_{S30}} = \frac{\phi_1}{V_{S30}} + \phi_2 \cdot \phi_3 \cdot \exp(V_{S30} - 360) \cdot \ln\left(\frac{SA_{1130} + \phi_4}{\phi_4}\right) \quad (5.3)$$

The variance of the site-dependent function that is a result of V_{S30} variance is then

$$\sigma_{\ln(SA)}^2 (\text{from } V_{S30}) = \sigma_{V_{S30}}^2 \left(\frac{\partial \ln(SA)}{\partial V_{S30}} \right) \quad (5.4)$$

As seen here in this basic form, propagating the uncertainty is a function of the variance of the independent term, in this case V_{S30} , and the sensitivity of the functional form to this independent term. Mean values for all the parameters were substituted, and the database average $COV \approx 27\%$ was used to calculate the variance that propagates through the model. The mean V_{S30} for the database varied from 406 m/s to 392 m/s with respect to the spectral ordinate. The mean spectral acceleration of rock, SA_{1130} , was calculated using Equation 5.1 with the mean values substituted. This propagated uncertainty was removed from the overall uncertainty as

$$\sigma_{\ln(SA)}^2 (\text{reduced}) = \sigma_{\ln(SA)}^2 - \sigma_{\ln(SA)}^2 (\text{from } V_{S30}) \quad (5.5)$$

The results of using FOSM, shown in Figure 5.4, are quite similar to the Bayesian regression results in trend and magnitude. This provides confidence in the results from both methods and lends to the use of FOSM as a simplified analysis when Bayesian regression is too time consuming and cumbersome.

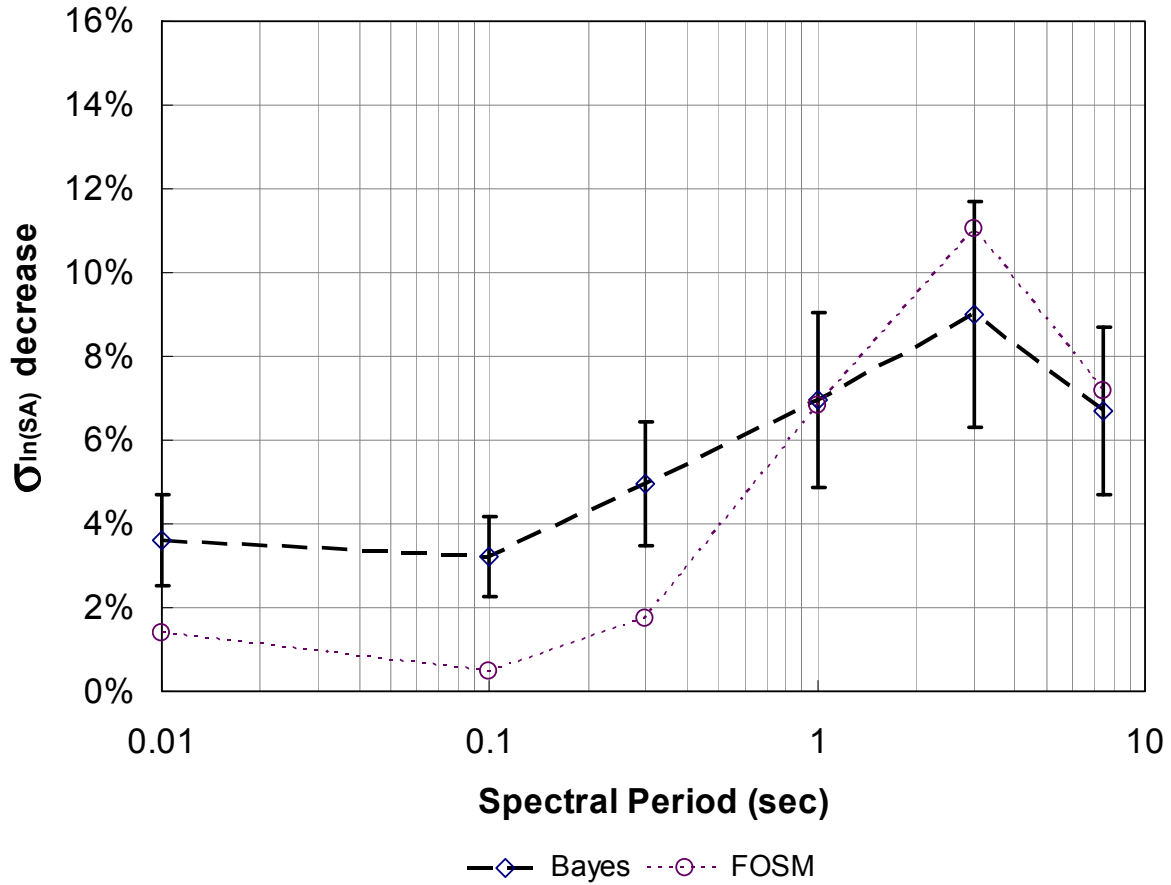


Fig. 5.4 First-order second-moment (FOSM) variance analysis results. These results compare favorably with Bayesian regression results, lending support to results of both methods and confirming that simplified methods provide reasonable results.

5.2.2 Monte Carlo Simulations

The second approximation method used to propagate the uncertainty through the ground motion prediction equation is Monte Carlo (MC) simulations. The ground motion prediction equation with mean values for the parameters is used along with a large number of randomly generated realizations of the inexact parameter of interest, V_{S30} . The statistics of the results show the variance of the model with respect to the variance of the randomly generated inexact generated. The $COV \approx 27\%$ was used with the mean value of V_{S30} for each spectral ordinate, and 100,000 simulations were generated. Each simulation was pushed through the prediction equation with a histogram with mean and standard deviation as the results. Figure 5.5 shows a comparison of MC with the previous Bayesian regression and FOSM results. There is generally good agreement between the FOSM and MC, showing the same trends: a slight drop from PGA to 0.1

sec, and a maximum at 3.0 sec with a subsequent drop. The magnitudes of the three methods are within the same range. For each spectral ordinate the approximate methods either under- or overestimate the Bayesian regression results, but the average percent decreases of the model standard deviation in natural units for the three methods are quite similar; Bayesian regression 5.7%, FOSM 4.8%, and MC 5.4%.

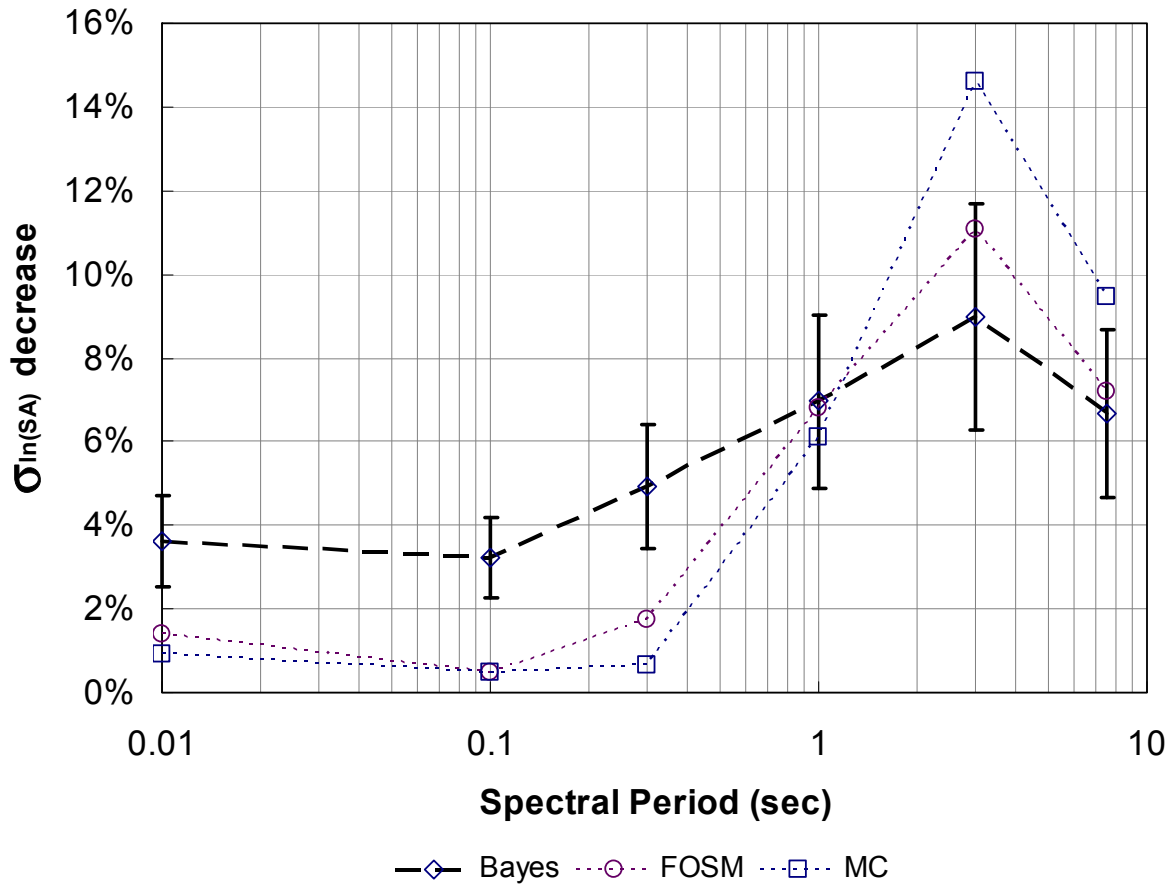


Fig. 5.5 Monte Carlo (MC) simulation results with respect to FOSM and Bayesian regression results. All three methods show similar general trends.

5.3 OTHER GROUND MOTION PREDICTION EQUATIONS

Ideally Bayesian regression, FOSM, and MC methods would be applied to all the NGA models to compare how V_{S30} uncertainty influences each one, the influence being a function of how each ground motion prediction equation mathematically treats the parameter. And ultimately the measurement uncertainty from each parameter (V_{S30} , M_w , and R) would be accounted for in this type of variance analysis. At this stage those tasks are still to be tackled. For comparison

purposes the Boore et al. (1997) ground motion prediction equation is readdressed using the same variance analysis techniques that were applied to Chiou and Youngs (2008). The results are limited to PGA because that is all the database information available from Boore et al. (1997). The results show a similar trend. The Bayesian regression results showed a 20% decrease in the standard deviation for PGA; FOSM showed no decrease; and MC showed a 4% decrease. Figure 5.4 shows that the MC results for PGA were a factor of 4 less than the Bayesian regression results, which agrees with the results using Boore et al. (1997). The FOSM results are curious in that no decrease was measured. This appears to be a by-product of the specific model formulation of Boore et al. (1997) and that this equation is linearly insensitive to V_{S30} for the PGA ordinate. This favorable comparison of the Bayesian regression and MC results using two different ground motion prediction equations provides additional confidence in the methodology and the usefulness of this type of variance analysis.

5.4 IMPACT OF RESULTS

Up to this point the discussion has focused on the technical aspects of performing variance analysis, in quantifying the parameter uncertainty, and in translating that uncertainty through ground motion prediction equations using different techniques. The discussion will now focus on the usefulness of this analysis by showing the impact of the results in engineering terms. Figure 5.6 is a plot of the lognormal probability density functions (PDFs) of the 0.01 sec (PGA) and 3.0 sec periods. The first curve is the PDF of the Chiou and Youngs (2008) results for the noted earthquake and site conditions, the second is the PDF that reflects the Bayesian regression results. The taller, narrower distribution of the Bayesian regression shows a reduced standard deviation which translates to more certainty in the ground motion measure.

The locations of the median plus one and two standard deviations noted as 1 sigma and 2 sigma, respectively, are also shown. The difference or spread of the 1 sigma and 2 sigma predictions demonstrates the impact and benefit of variance analysis. A more accurate estimate of the seismic demand is afforded through variance analysis, which becomes particularly important for rarer events that fall to the right of the median. This can be important for critical or long-lived structures that are designed for long-return periods (e.g., 2500 year events or greater). An example where this might have a dramatic impact is the Yucca Mountain project, where the 10,000 year event is considered within the design life. The plots account for parameter

uncertainty in only V_{S30} . Further research will include the parameter uncertainty in both M_w and R , which will narrow the distribution further and result in even better estimates of the rarer events.

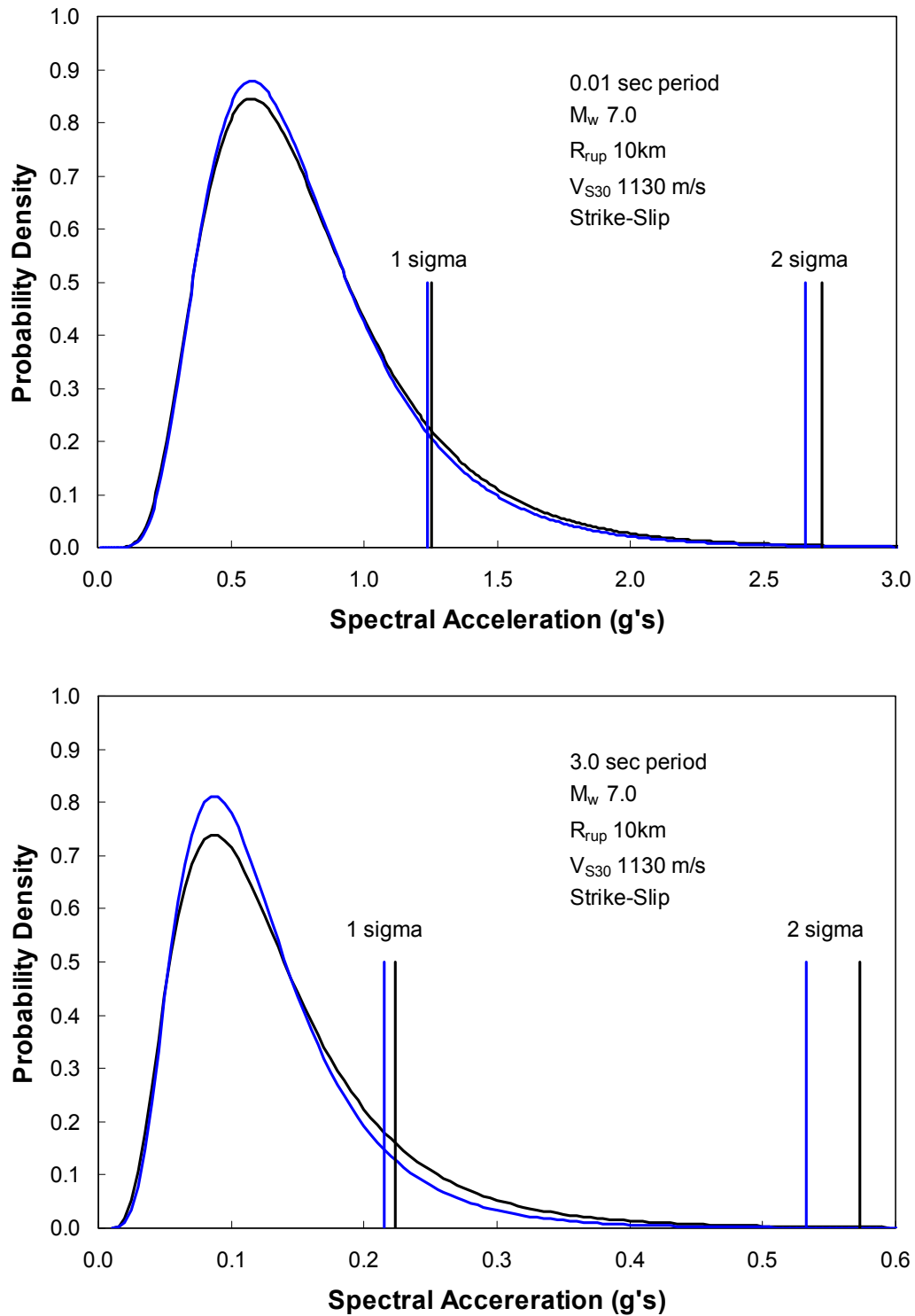


Fig. 5.6 Chiou and Youngs (2008) probability density function predictions for PGA and 3.0 sec period, given earthquake, distance, and site conditions compared to probability density function that accounts for parameter uncertainty in V_{S30} . Difference in 1 sigma and 2 sigma results demonstrates the impact of variance analysis on ground motion prediction of rarer events.

6 Summary and Conclusions

This report is the culmination of several years of research into the variance analysis of ground motion prediction equations. The goal was to account for parameter uncertainty of the independent variables and to demonstrate how through Bayesian regression a better estimate of the dependent variable can be achieved. This report documents the mathematical formulation of the Bayesian regression technique used. A feasibility study was conducted in the early phase of the research to verify that the technique would produce useful results. Research efforts were invested in quantifying the parameter uncertainty of the independent variables, with V_{S30} receiving the bulk of the attention. Finally an NGA model was used as the limit-state function, and the parameter uncertainty of V_{S30} was accounted for using Bayesian regression, which resulted in a more accurate assessment of NGA model uncertainty. Two approximate solution methods were evaluated against the Bayesian regression results and provided reasonable average results, which affords simplified methods for evaluating the impact of parameter uncertainty. A more accurate assessment of model uncertainty is particularly important in an engineering sense for rarer, or long-return period, events, the types that can dominate the design of critical structures with a long design life. Future research endeavors will evaluate other NGA models using Bayesian regression, and further quantify the parameter uncertainty of M_w and R so that these two independent variables can be accounted for in the Bayesian regression.

REFERENCES

- Abrahamson, N. A., and Shedlock, K. M. (1997). "Overview." *Seismological Research Letters*, 68(1).
- Abrahamson, N. A., and Silva, W. J. (1997). "Empirical Response Spectral Attenuation Relations for Shallow Crustal Earthquakes." *Seismological Research Letters*, 68(1).
- Ang, A. H-S., and Tang, W. H. (1975) Probability concepts in Engineering Planning and Design, Volume 1. Wiley, New York.
- Asten, M. W., and Boore, D. M. (2005). "Comparison of Shear-Velocity Profiles of Unconsolidated Sediments near the Coyote Borehole (CCOC) Measured with Fourteen Invasive and Non-Invasive Methods." USGS OFR 2005-1169.
- Boore, D. M. (2006). "Determining Subsurface Shear-Wave Velocities: A Review." *ESG2006, 3rd International Symposium on the Effect of Surface Geology on Seismic Motion*, Grenoble, France, Paper No: 103.
- Boore, D. M., Joyner, W. B., and Fumal, T. E. (1997). "Equations for Estimating Horizontal Response Spectra and Peak Acceleration from Western North American Earthquakes: A Summary of Recent Work." *Seismological Research Letters*, 68(1).
- Box, G. E. P., and Tao, G. C. (1992). *Bayesian Inference in Statistical Analysis.*, John Wiley and Sons, Inc.
- Brown, L. T., Boore, D. M., and Stokoe, K. H. I. (2002). "Comparison of Shear Wave Slowness Profiles at 10 Strong-Motion Sites from Noninvasive SASW Measurements and Measurements Made in Boreholes." *Bulletin of Seismological Society of America*, 92(8), 3116-3133.
- BSSC-Building Seismic Safety Council (2001). NEHRP recommended provisions for seismic regulations for new buildings and other structures, 2000 Edition, Part I: Provisions, prepared by the BSSC for the Federal Emergency management Agency, FEMA Report 368, Washington, D.C.
- Campbell, K. W., and Bozorgnia, Y. (2003). "Updated Near-Source Ground-Motion (Attenuation) Relations for the Horizontal and Vertical Components of Peak Ground Acceleration and Acceleration Response Spectra." *Bulletin of Seismological Society of America*, 93(1).
- Chiou, B. S.-J., and Youngs, R. R. (2006). "PEER-NGA Empirical Ground Motion Model for the Average Horizontal Component of Peak Acceleration and Pseudo-Spectral Acceleration for Spectral Periods of 0.01 to 10 Seconds." Pacific Earthquake Engineering Research Center. http://peer.berkeley.edu/products/Chiou_Youngs_NGA_2006.html
- Chiou, B., and Youngs, R. R. (2008). "An NGA Model for the Average Horizontal Component of Peak Ground Motion and Response Spectra." *Earthquake Spectra*, 24(1), 173-215.
- Chiou, B., Darragh, R., Gregor, N., and Silva, W. (2008). "NGA Project Strong-Motion Database." *Earthquake Spectra*, 24(1), 23-44.
- Dai, S.-H., and Wang, M.-O. (1992). *Reliability Analysis in Engineering Applications*, Van Nostrand Reinhold, New York.
- Der Kiureghian, A. (2000). "A Bayesian Framework for Fragility Assessment." Applications of Statistic and Probability-Civil Engineering Reliability Risk Analysis, R. E. Melchers and M. G. Stewart, eds., Balkema, Rotterdam, 1003-1101.
- EPRI-Electric Power Research Institute. (1993). "Guidelines for determining design basis ground motions. Vol. 3: Appendices for field investigations." *EPRI TR-102293*, , Palo Alto, CA.

- Gardoni, P. (2002). "Probabilistic models and fragility estimates for structural components and systems,," Ph.D. dissertation, University of California Berkeley.
- Gardoni, P., Der Kiureghian, A., and Mosalam, K. M. (2002). "Probabilistic Capacity Models and Fragility Estimates for Reinforced Concrete Columns based on Experimental Observations." *Journal of Engineering Mechanics*, October.
- Hardin, B. O. (1978). "The nature of stress-strain behavior of soils." *Proc. Earthquake Engineering and Soil Dynamics, Pasadena, CA*.
- Harp, E. L., Jibson, R. W., Kayen, R. E., Keefer, D. K., Sherrod, B. S., Carver, G. A., Collins, B. D., Moss, R. E. S., and Sitar, N. S. (2003). "Landslides and Liquefaction Triggered by the M7.9 Denali Fault Earthquake of 3 November 2002." *GSA Today*, 13(8).
- Humphries, W. K., and Wahls, H. E. (1968). "Stress history effects on dynamic modulus of clay." *Journal of Soil Mechanics, Foundation Division ASCE*, 94(SM2), 371-389.
- Hunt, C. E., Pestana, J. M., Bray, J. D., and Riemer, M. F. (2002). "Effect of Pile Driving on Static and Dynamic Properties of Soft Clay." *Journal of Geotechnical and Geoenvironmental Engineering*, 128(1), 13-24.
- Isaaks, E.H., and Srivastava, R.M. (1989). *Applied Geostatistics*. Oxford University Press, New York.
- Jamiołkowski, M., Leroueil, S., and LoPresti, D. C. F. (1991). "Theme Lecture: Design parameters from theory to practice." *Proc. Geo-Coast 91, Yokohama, Japan*, 1-41.
- Jaume, S. C. (2006). "Shear Wave Velocity Profiles via Seismic Cone Penetration Test and Refraction Microtremor Techniques at ANSS Strong Motion Sites in Charleston, South Carolina." *Seismological Research Letters*, 77(6), 771-779.
- Kalinski, M. E., and Stokoe, K. H. I. (2003). "In Situ Estimate of Shear Wave Velocity Using Borehole Spectral Analysis of Surface Waves Tool." *Journal of Geotechnical and Geoenvironmental Engineering*, 129(6), 529-535.
- Kulhawy, F.H., and Mayne, P.W. (1990). "Manual on Estimating Soil Properties for Foundation Design." EPRI Report EL-6800.
- Liu, H.-P., Boore, D. M., Joyner, W. B., Oppenheimer, D. H., Warrick, R. E., Zhang, W., Hamilton, J. C., and Brown, L. T. (2000). "Comparison of phase velocities from array measurements of rayleigh waves associated with microtremor and results calculated from borehole shear-wave velocity profiles." *Bulletin of Seismological Society of America*, 90(3), 666-678.
- Louie, J. N. (2001). "Faster, Better: Shear-Wave Velocity to 100 Meters Depth from Refraction Microtremor Arrays." *Bulletin of Seismological Society of America*, 91(2), 347-364.
- Lunne, T., Robertson, P. K., and Powell, J. J. M. (1997). *Cone Penetration Testing in Geotechnical Practice*, Blackie Academic & Professional, New York.
- Marosi, K. T., and Hiltunen, D. R. (2004). "Characterization of Spectral Analysis of Surface Waves Shear Wave Velocity Measurement Uncertainty." *Journal of Geotechnical and Geoenvironmental Engineering*, 130(10), 1034-1041.
- Martin, A. J., and Diehl, J. G. (2004). "Practical experience using a simplified procedure to measure average shear-wave velocity to a depth of 30 meters (V_{S30})." *13th World Conf. on Earthquake Engineering*, Vancouver, B.C., Canada.
- Moss, R. E. S. (2008). "Quantifying Measurement Uncertainty Associated with Thirty Meter Shear Wave Velocity (V_{S30})." *Bulletin of Seismological Society of America*, 98(3).

- Moss, R. E. S., and Der Kiureghian, A. (2006). "Incorporating Parameter Uncertainty into Attenuation Relationships." *8th U.S. National Conference on Earthquake Engineering*, San Francisco.
- Moss, R. E. S., and Der Kiureghian, A. (2006). "Incorporating Parameter Uncertainty into Attenuation Relationships." *8th U.S. National Conference on Earthquake Engineering*, San Francisco.
- Moss, R. E. S., Cetin, K. O., and Seed, R. B. (2003). "Seismic Liquefaction Triggering Correlations within a Bayesian Framework ." *9th International Conf. Application of Statistic and Probability in Civil Engineering*, Berkeley.
- Rix, G. J., Hebler, G. L., and Orozco, M. C. (2002). "Near-surface Vs profiling in the New Madrid seismic zone using surface-wave methods." *Seismological Research Letters*, 73(3), 380-392.
- Scherbaum, F., Schmedes, J., and Cotton, F. (2004). "On the Conversion of Source-to-Site Distance Measures for Extended Earthquake Source Models." *Bulletin of Seismological Society of America*, 94(3), 1053-1069.
- Stephenson, W. J., Louie, J. N., Pullammanappallil, S., Williams, R. A., and Odum, J. K. (2005). "Blind shear-wave velocity comparison of ReMi and MASW results with boreholes to 200 m in Santa Clara Valley: Implications for earthquake ground-motion assessment." *Bulletin of Seismological Society of America*, 95, 2506-2516.
- Thelen, W. A., Clark, M., Lopez, C. T., Loughner, C., Park, H., Scott, J. B., Smith, S. B., Greschke, B., and Louie, J. N. (2006). "A transect of 200 shallow shear velocity profiles across the Los Angeles Basin." *Bulletin of Seismological Society of America*, in press.
- Thompson, E. M., Baise, L. G., and Kayen, R. E. (2007). "Spatial correlation of shear-wave velocity in the San Francisco Bay Area sediments." *Soil Dynamics and Earthquake Engineering*, 27, 144-152.
- Thompson, E.M., Baise, L.G., and Kayen, R.E. (2007). "Spatial correlation of shear-wave velocity in the San Francisco Bay Area sediments." *Soil Dynamics and Earthquake Engineering*, 27, 144-152.
- Williams, R. A., Stephenson, W. J., and Odum, J. K. (2003). "Comparison of P- and S-wave velocity profiles obtained from surface seismic refraction/reflection and downhole data." *Tectonophysics*, 368, 71-88.
- Wills, C. J., and Clahan, K. B. (2004). "NGA: Site Condition Metadata from Geology." *Project 1L05*, Pacific Earthquake Engineering Research Institute.
- Wills, C. J., and Silva, W. (1998). "Shear-Wave Velocity Characteristics of Geologic Units in California." *Earthquake Spectra*, 14(3), 533-556.
- Xia, J., Miller, R. D., Park, C. B., Hunter, J. A., Harris, J. B., and Ivanov, J. (2002). "Comparing shear-wave velocity profiles inverted from multichannel surface wave with borehole measurements." *Soil Dynamics and Earthquake Engineering*, 22, 181-190.

Appendix

MatLab code for Bayesian regression procedure using a simple linear example.

```
%%%%%%%%%%%%%%%%%%%%%%%%%%%%%%%%%%%%%%%%%%%%%%%%%%%%%%%%%%%%%%%%%%%%%%%%%
% Using Bayes Framwork to perform linear regression with
% example from Ang and Tang (1975) E71 p290-291
%
%%%%%%%%%%%%%%%%%%%%%%%%%%%%%%%%%%%%%%%%%%%%%%%%%%%%%%%%%%%%%%%%%%%%%%%%%
%
% Importance sampling is used in this program
% to carry out the necessary integrations over the Bayesian kernel. The
% joint lognormal distribution with specified means, standard deviations
% and correlation matrix is used for the sampling distribution.
% Convergence will be faster if the statistics of the sampling
% distribution are close to the corresponding statistics of the
% posterior distribution that are to be computed. The program may be
% run several times to adjust the statistics of the sampling distribution.
%
% For numerical stability, it is important that the normalizing factor
% k in the Bayesian updating formula be neither too small nor too large.
% This factor can be adjusted by scaling the likelihood function. In this
% program this is done by adjusting the "scale" parameter.
%
% Run the program with trial estimates of the means, standard deviation
% and correlation matrix of the sampling density, and of the scale
% parameter. This will give a first estimate of the reciprocal of the
% normalizing factor k and the posterior statistics of the parameters.
% A good first estimate for the sampling mean is the argmax(g(x)), and
% a good first sampling correlation matrix is the inverse of the Hessian.
% Make sure that the sampling density has sufficiently large standard
% deviations (no smaller than the posterior standard deviations estimated).
% Use the first posterior estimates as the new means, standard deviations
% and correlation matrix of the sampling distribution and adjust the
% scale parameter (decrease it if k is too large, increase it if k is too
% small). Run the program again to obtain a 2nd set of posterior estimates.
% Repeat this process until sufficient accuracy in the posterior estimates
% is achieved.
%
% The accuracy is measured in terms of the coefficients of variation of
% the posterior mean estimates (denoted cov_p_mean in this program).
% A value less than 25% for each element of cov_p_mean is a good level
% of accuracy.
%
% The results of the computation are stored in the file "Results2.mat"
% as follows:
%
```



```

%      nmin    minimum number of simulations
%      nmax    maximum number of simulations
%      npar    number of parameters
%      k       normalizing factor in the updating formula
%      p_mean  posterior mean vector
%      cov_p_mean  c.o.v. of the posterior mean estimates
%      p_st_dev  vector of posterior standard deviations
%      p_cov   vector of posterior c.o.v.'s
%      p_cor   posterior correlation matrix
%
%%%%%%%%%%%%%%%%%%%%%%%%%%%%%%%%%%%%%%%%%%%%%%%%%%%%%%%%%%%%%%%%%%%%%%%%%%

clear all;
load E71data.mat; %Data from Ang and Tang example E71 (see below)
tic;
disp(' ');
disp('updating.....please wait');

errDepth=0.10.*Depth; %COV of Depth 10%

%----- Specify the means, standard deviations and correlation matrix
%----- of the sampling density

M = [0.0517
     -0.0029
      0.200];

D = [0.01      0.0000   0.0000
     0.0000    0.03     0.0000
     0.0000    0.0000   0.09  ];

R = [1.0000    0.6839   -0.1591
     0.6839    1.0000   -0.0334
    -0.1591   -0.0334    1.0000];

%----- Specify the scale parameter

scale = .01;

%----- Specivy the c.o.v. for convergence

convergence = 0.50;

%----- Set minimum and maximum number of simulations:

nmin = 50;
nmax = 100000;

%----- Begin calculations

d = diag(D); % vector of standard deviations
cov = d ./ M; % c.o.v.'s
z = sqrt(log(1+(cov).^2)); % zeta parameters of lognormal distribution
LAM = log(M) - 0.5 * (z).^2; % lambda parameters of lognormal dist.
Z = diag(z); % diagonal matrix of zeta's

```

```

S = Z*R*Z; % covariance matrix of transformed normals
L= chol(S)'; % lower choleski decomposition of S
iS = inv(S); % inverse of S

%----- Initialize integral values:
I1 = 0;
I2 = 0;
I3 = 0;
I4 = 0;

npar = length(M); % number of parameters
ndata = length(Strength); % number of ordinates
i_counter = 0;
flag = 1;
constant = 1/( (6.28318531)^(npar/2) * sqrt(det(S)) );

%----- Begin importance sampling:

for i = 1:nmax

    %-- simulate standard normal random variables;
    u = randn(npar,1);
    theta = exp( LAM + L*u); % simulated lognormal theta's

    %-- define three kernels
    K1 = 1; % this is for computing the normalizing constant k
    K2 = theta; % this is for computing the mean
    K3 = theta*theta'; % this is for computing the mean squares

    %-- initialize product functions
    lhood = 1;

    %-- compute likelihood function
    g = theta(1).*Depth - theta(2);
    errg = Strength-g;

    for k = 1:ndata
        sq_std(k) = theta(3)^2 + theta(1)^2*errDepth(k)^2;
        norm_value(k) = errg(k)/sqrt(sq_std(k));
        value(k) = normpdf(norm_value(k)).*sign(norm_value(k));
        lhood = exp(log((lhood*value(k))/sqrt(sq_std(k))))+scale);
    end

    %-- compute the prior distribution (non-informative):
    p = 1/(theta(1)*theta(2)*theta(3));

    %-- compute the sampling probability density
    h = constant * exp(-0.5*(log(theta)-LAM)'*iS*(log(theta)-LAM));
    h = h/(theta(1)*theta(2)*theta(3));

    %-- compute (kernel*likelihood*prior)/sampling-density:
    I1 = I1 + K1*lhood*p/h;
    I2 = I2 + K2.*lhood.*p/h;
    I3 = I3 + K3*lhood*p/h;
    I4 = I4 + (K2.*lhood.*p/h).^2; % this is for computing cov_p_mean

```

```

%--- reciprocal of the normalizing constant
k = I1/i;

%--- posterior mean and its c.o.v.
p_mean = I2/I1;
cov_p_mean = sqrt(( 1/i*(I4/(k.^2*i) - (I2/(k*i)).^2) )) ./abs(p_mean);

%--- posterior covariance matrix
p_cov = I3/I1 - p_mean*p_mean';

% check if c.o.v is <= convergence for all the posterior means, but
% make sure that at least nmin simulations are performed.
% flag = 0 means that convergence has been achieved.

i_counter = i_counter+1;
if max(cov_p_mean) <= convergence & i_counter>nmin
flag = 0;
break
end
end

toc;
t=toc/60;

%----- display results:
beep;
disp('--- Number of simulations')
disp(i_counter);

disp('--- Number of parameters')
disp(npar);

disp('--- Run time (min)')
disp(t);

disp('===== Bayesian Posterior Estimates =====')

disp('--- Reciprocal of normalizing factor k')
disp(real(k));

disp('--- Posterior means')
disp(real(p_mean));

disp('--- c.o.v.s for the posterior means')
disp(real(cov_p_mean))

for i=1:npar
    p_st_dev(i) = sqrt(p_cov(i,i));
    p_c_o_v(i) = p_st_dev(i)/abs(p_mean(i));
end
disp('--- Posterior standard deviations')
disp(real(p_st_dev))

```

```

disp('--- Posterior c.o.v.s')
disp(real(p_c_o_v))
for i=1:npar
    for j=1:npar
        p_cor(i,j)=p_cov(i,j)/(p_st_dev(i)*p_st_dev(j));
    end
end
disp('--- Posterior correlation matrix')
disp(real(p_cor));

%plotting mean results against linear regression results
x=Depth;
y=0.0515*x+0.029; %linear regresssion coefficients
y_prime=p_mean(1).*x-p_mean(2);
y_plus=y+0.192;
y_minus=y-0.192;
y_prime_plus=y_prime+p_mean(3);
y_prime_minus=y_prime-p_mean(3);
plot(Strength,-Depth,'o',y,-x,'g',y_prime,-x,'r',y_plus,-x,'--g',y_minus,-
x,'--g',y_prime_plus,-x,'--r',y_prime_minus,-x,'--r');

```

Data file containing E71data.mat

```
>> load E71data.mat
```

```
>> who
```

Your variables are:

```
Depth    Strength  errDepth  errStrength
```

```
>> Depth'
```

```
ans =
```

```
6  8  14  14  18  20  20  24  28  30
```

```
>> Strength'
```

ans =

0.2800 0.5800 0.5000 0.8300 0.7100 1.0100 1.2900 1.5000 1.2900 1.5800

>> errDepth'

ans =

3 4 7 7 9 10 115 12 14 15

>> errStrength'

ans =

0.0840 0.1740 0.1500 0.2490 0.2130 0.3030 0.3870 0.4500 0.3870 0.4740

Linear Regression Example Results

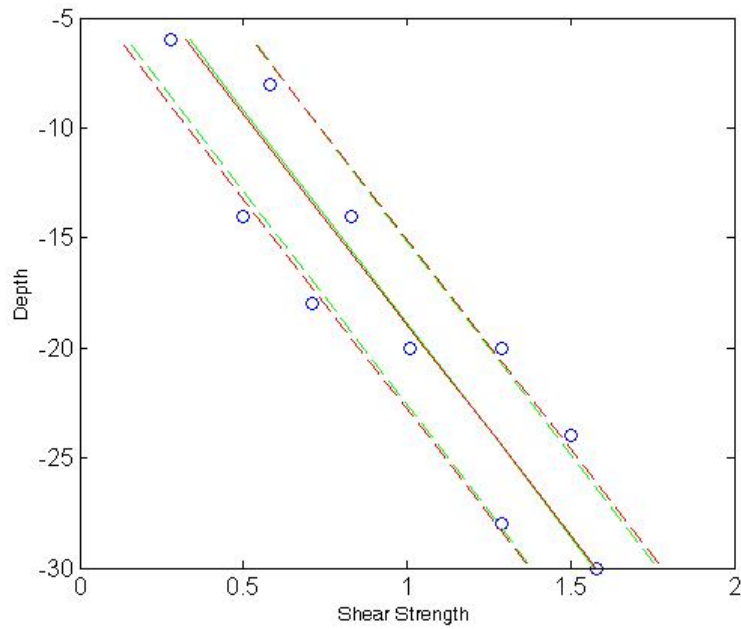


Fig. A1 Bayesian regression results that mimic “classic” regression results using Ang and Tang E71 example. Median and plus and minus standard deviation lines are shown along with data.

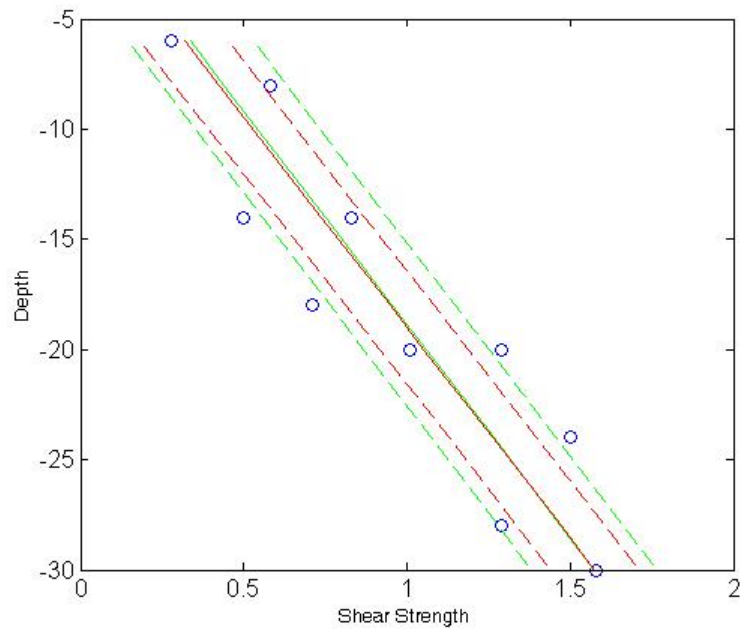


Fig. A2 Bayesian regression results where parameter uncertainty of depth is taken into account. Reduced model uncertainty is realized by including parameter uncertainty.

PEER REPORTS

PEER reports are available individually or by yearly subscription. PEER reports can be ordered at http://peer.berkeley.edu/publications/peer_reports.html or by contacting the Pacific Earthquake Engineering Research Center, 1301 South 46th Street, Richmond, CA 94804-4698. Tel.: (510) 665-3448; Fax: (510) 665-3456; Email: peer_editor@berkeley.edu

- PEER 2009/02** *Improving Earthquake Mitigation through Innovations and Applications in Seismic Science, Engineering, Communication, and Response. Proceedings of a U.S.-Iran Seismic Workshop.* October 2009.
- PEER 2009/01** *Evaluation of Ground Motion Selection and Modification Methods: Predicting Median Interstory Drift Response of Buildings.* Curt B. Haselton, Ed. June 2009.
- PEER 2008/10** *Technical Manual for Strata.* Albert R. Kottke and Ellen M. Rathje. February 2009.
- PEER 2008/09** *NGA Model for Average Horizontal Component of Peak Ground Motion and Response Spectra.* Brian S.-J. Chiou and Robert R. Youngs. November 2008.
- PEER 2008/08** *Toward Earthquake-Resistant Design of Concentrically Braced Steel Structures.* Patxi Uriz and Stephen A. Mahin. November 2008.
- PEER 2008/07** *Using OpenSees for Performance-Based Evaluation of Bridges on Liquefiable Soils.* Stephen L. Kramer, Pedro Arduino, and HyungSuk Shin. November 2008.
- PEER 2008/06** *Shaking Table Tests and Numerical Investigation of Self-Centering Reinforced Concrete Bridge Columns.* Hyung IL Jeong, Junichi Sakai, and Stephen A. Mahin. September 2008.
- PEER 2008/05** *Performance-Based Earthquake Engineering Design Evaluation Procedure for Bridge Foundations Undergoing Liquefaction-Induced Lateral Ground Displacement.* Christian A. Ledezma and Jonathan D. Bray. August 2008.
- PEER 2008/04** *Benchmarking of Nonlinear Geotechnical Ground Response Analysis Procedures.* Jonathan P. Stewart, Annie On-Lei Kwok, Youssef M. A. Hashash, Neven Matasovic, Robert Pyke, Zhiliang Wang, and Zhaohui Yang. August 2008.
- PEER 2008/03** *Guidelines for Nonlinear Analysis of Bridge Structures in California.* Ady Aviram, Kevin R. Mackie, and Božidar Stojadinović. August 2008.
- PEER 2008/02** *Treatment of Uncertainties in Seismic-Risk Analysis of Transportation Systems.* Evangelos Stergiou and Anne S. Kiremidjian. July 2008.
- PEER 2008/01** *Seismic Performance Objectives for Tall Buildings.* William T. Holmes, Charles Kircher, William Petak, and Nabih Youssef. August 2008.
- PEER 2007/12** *An Assessment to Benchmark the Seismic Performance of a Code-Conforming Reinforced Concrete Moment-Frame Building.* Curt Haselton, Christine A. Goulet, Judith Mitrani-Reiser, James L. Beck, Gregory G. Deierlein, Keith A. Porter, Jonathan P. Stewart, and Ertugrul Taciroglu. August 2008.
- PEER 2007/11** *Bar Buckling in Reinforced Concrete Bridge Columns.* Wayne A. Brown, Dawn E. Lehman, and John F. Stanton. February 2008.
- PEER 2007/10** *Computational Modeling of Progressive Collapse in Reinforced Concrete Frame Structures.* Mohamed M. Talaat and Khalid M. Mosalam. May 2008.
- PEER 2007/09** *Integrated Probabilistic Performance-Based Evaluation of Benchmark Reinforced Concrete Bridges.* Kevin R. Mackie, John-Michael Wong, and Božidar Stojadinović. January 2008.
- PEER 2007/08** *Assessing Seismic Collapse Safety of Modern Reinforced Concrete Moment-Frame Buildings.* Curt B. Haselton and Gregory G. Deierlein. February 2008.
- PEER 2007/07** *Performance Modeling Strategies for Modern Reinforced Concrete Bridge Columns.* Michael P. Berry and Marc O. Eberhard. April 2008.
- PEER 2007/06** *Development of Improved Procedures for Seismic Design of Buried and Partially Buried Structures.* Linda Al Atik and Nicholas Sitar. June 2007.
- PEER 2007/05** *Uncertainty and Correlation in Seismic Risk Assessment of Transportation Systems.* Renee G. Lee and Anne S. Kiremidjian. July 2007.
- PEER 2007/04** *Numerical Models for Analysis and Performance-Based Design of Shallow Foundations Subjected to Seismic Loading.* Sivapalan Gajan, Tara C. Hutchinson, Bruce L. Kutter, Prishati Raychowdhury, José A. Ugalde, and Jonathan P. Stewart. May 2008.
- PEER 2007/03** *Beam-Column Element Model Calibrated for Predicting Flexural Response Leading to Global Collapse of RC Frame Buildings.* Curt B. Haselton, Abbie B. Liel, Sarah Taylor Lange, and Gregory G. Deierlein. May 2008.

- PEER 2007/02** *Campbell-Bozorgnia NGA Ground Motion Relations for the Geometric Mean Horizontal Component of Peak and Spectral Ground Motion Parameters.* Kenneth W. Campbell and Yousef Bozorgnia. May 2007.
- PEER 2007/01** *Boore-Atkinson NGA Ground Motion Relations for the Geometric Mean Horizontal Component of Peak and Spectral Ground Motion Parameters.* David M. Boore and Gail M. Atkinson. May. May 2007.
- PEER 2006/12** *Societal Implications of Performance-Based Earthquake Engineering.* Peter J. May. May 2007.
- PEER 2006/11** *Probabilistic Seismic Demand Analysis Using Advanced Ground Motion Intensity Measures, Attenuation Relationships, and Near-Fault Effects.* Polsak Tothong and C. Allin Cornell. March 2007.
- PEER 2006/10** *Application of the PEER PBEE Methodology to the I-880 Viaduct.* Sashi Kunnath. February 2007.
- PEER 2006/09** *Quantifying Economic Losses from Travel Forgone Following a Large Metropolitan Earthquake.* James Moore, Sungbin Cho, Yue Yue Fan, and Stuart Werner. November 2006.
- PEER 2006/08** *Vector-Valued Ground Motion Intensity Measures for Probabilistic Seismic Demand Analysis.* Jack W. Baker and C. Allin Cornell. October 2006.
- PEER 2006/07** *Analytical Modeling of Reinforced Concrete Walls for Predicting Flexural and Coupled-Shear-Flexural Responses.* Kutay Orakcal, Leonardo M. Massone, and John W. Wallace. October 2006.
- PEER 2006/06** *Nonlinear Analysis of a Soil-Drilled Pier System under Static and Dynamic Axial Loading.* Gang Wang and Nicholas Sitar. November 2006.
- PEER 2006/05** *Advanced Seismic Assessment Guidelines.* Paolo Bazzurro, C. Allin Cornell, Charles Menun, Maziar Motahari, and Nicolas Luco. September 2006.
- PEER 2006/04** *Probabilistic Seismic Evaluation of Reinforced Concrete Structural Components and Systems.* Tae Hyung Lee and Khalid M. Mosalam. August 2006.
- PEER 2006/03** *Performance of Lifelines Subjected to Lateral Spreading.* Scott A. Ashford and Teerawut Juirnarongrit. July 2006.
- PEER 2006/02** *Pacific Earthquake Engineering Research Center Highway Demonstration Project.* Anne Kiremidjian, James Moore, Yue Yue Fan, Nesrin Basoz, Ozgur Yazali, and Meredith Williams. April 2006.
- PEER 2006/01** *Bracing Berkeley. A Guide to Seismic Safety on the UC Berkeley Campus.* Mary C. Comerio, Stephen Tobriner, and Ariane Fehrenkamp. January 2006.
- PEER 2005/16** *Seismic Response and Reliability of Electrical Substation Equipment and Systems.* Junho Song, Armen Der Kiureghian, and Jerome L. Sackman. April 2006.
- PEER 2005/15** *CPT-Based Probabilistic Assessment of Seismic Soil Liquefaction Initiation.* R. E. S. Moss, R. B. Seed, R. E. Kayen, J. P. Stewart, and A. Der Kiureghian. April 2006.
- PEER 2005/14** *Workshop on Modeling of Nonlinear Cyclic Load-Deformation Behavior of Shallow Foundations.* Bruce L. Kutter, Geoffrey Martin, Tara Hutchinson, Chad Harden, Sivapalan Gajan, and Justin Phalen. March 2006.
- PEER 2005/13** *Stochastic Characterization and Decision Bases under Time-Dependent Aftershock Risk in Performance-Based Earthquake Engineering.* Gee Liek Yeo and C. Allin Cornell. July 2005.
- PEER 2005/12** *PEER Testbed Study on a Laboratory Building: Exercising Seismic Performance Assessment.* Mary C. Comerio, editor. November 2005.
- PEER 2005/11** *Van Nuys Hotel Building Testbed Report: Exercising Seismic Performance Assessment.* Helmut Krawinkler, editor. October 2005.
- PEER 2005/10** *First NEES/E-Defense Workshop on Collapse Simulation of Reinforced Concrete Building Structures.* September 2005.
- PEER 2005/09** *Test Applications of Advanced Seismic Assessment Guidelines.* Joe Maffei, Karl Telleen, Danya Mohr, William Holmes, and Yuki Nakayama. August 2006.
- PEER 2005/08** *Damage Accumulation in Lightly Confined Reinforced Concrete Bridge Columns.* R. Tyler Ranf, Jared M. Nelson, Zach Price, Marc O. Eberhard, and John F. Stanton. April 2006.
- PEER 2005/07** *Experimental and Analytical Studies on the Seismic Response of Freestanding and Anchored Laboratory Equipment.* Dimitrios Konstantinidis and Nicos Makris. January 2005.
- PEER 2005/06** *Global Collapse of Frame Structures under Seismic Excitations.* Luis F. Ibarra and Helmut Krawinkler. September 2005.
- PEER 2005/05** *Performance Characterization of Bench- and Shelf-Mounted Equipment.* Samit Ray Chaudhuri and Tara C. Hutchinson. May 2006.

- PEER 2005/04** *Numerical Modeling of the Nonlinear Cyclic Response of Shallow Foundations.* Chad Harden, Tara Hutchinson, Geoffrey R. Martin, and Bruce L. Kutter. August 2005.
- PEER 2005/03** *A Taxonomy of Building Components for Performance-Based Earthquake Engineering.* Keith A. Porter. September 2005.
- PEER 2005/02** *Fragility Basis for California Highway Overpass Bridge Seismic Decision Making.* Kevin R. Mackie and Božidar Stojadinović. June 2005.
- PEER 2005/01** *Empirical Characterization of Site Conditions on Strong Ground Motion.* Jonathan P. Stewart, Yoojoong Choi, and Robert W. Graves. June 2005.
- PEER 2004/09** *Electrical Substation Equipment Interaction: Experimental Rigid Conductor Studies.* Christopher Stearns and André Filiatrault. February 2005.
- PEER 2004/08** *Seismic Qualification and Fragility Testing of Line Break 550-kV Disconnect Switches.* Shakhzod M. Takhirov, Gregory L. Fenves, and Eric Fujisaki. January 2005.
- PEER 2004/07** *Ground Motions for Earthquake Simulator Qualification of Electrical Substation Equipment.* Shakhzod M. Takhirov, Gregory L. Fenves, Eric Fujisaki, and Don Clyde. January 2005.
- PEER 2004/06** *Performance-Based Regulation and Regulatory Regimes.* Peter J. May and Chris Koski. September 2004.
- PEER 2004/05** *Performance-Based Seismic Design Concepts and Implementation: Proceedings of an International Workshop.* Peter Fajfar and Helmut Krawinkler, editors. September 2004.
- PEER 2004/04** *Seismic Performance of an Instrumented Tilt-up Wall Building.* James C. Anderson and Vitelmo V. Bertero. July 2004.
- PEER 2004/03** *Evaluation and Application of Concrete Tilt-up Assessment Methodologies.* Timothy Graf and James O. Malley. October 2004.
- PEER 2004/02** *Analytical Investigations of New Methods for Reducing Residual Displacements of Reinforced Concrete Bridge Columns.* Junichi Sakai and Stephen A. Mahin. August 2004.
- PEER 2004/01** *Seismic Performance of Masonry Buildings and Design Implications.* Kerri Anne Taeko Tokoro, James C. Anderson, and Vitelmo V. Bertero. February 2004.
- PEER 2003/18** *Performance Models for Flexural Damage in Reinforced Concrete Columns.* Michael Berry and Marc Eberhard. August 2003.
- PEER 2003/17** *Predicting Earthquake Damage in Older Reinforced Concrete Beam-Column Joints.* Catherine Pagni and Laura Lowes. October 2004.
- PEER 2003/16** *Seismic Demands for Performance-Based Design of Bridges.* Kevin Mackie and Božidar Stojadinović. August 2003.
- PEER 2003/15** *Seismic Demands for Nondeteriorating Frame Structures and Their Dependence on Ground Motions.* Ricardo Antonio Medina and Helmut Krawinkler. May 2004.
- PEER 2003/14** *Finite Element Reliability and Sensitivity Methods for Performance-Based Earthquake Engineering.* Terje Haukaas and Armen Der Kiureghian. April 2004.
- PEER 2003/13** *Effects of Connection Hysteretic Degradation on the Seismic Behavior of Steel Moment-Resisting Frames.* Janise E. Rodgers and Stephen A. Mahin. March 2004.
- PEER 2003/12** *Implementation Manual for the Seismic Protection of Laboratory Contents: Format and Case Studies.* William T. Holmes and Mary C. Comerio. October 2003.
- PEER 2003/11** *Fifth U.S.-Japan Workshop on Performance-Based Earthquake Engineering Methodology for Reinforced Concrete Building Structures.* February 2004.
- PEER 2003/10** *A Beam-Column Joint Model for Simulating the Earthquake Response of Reinforced Concrete Frames.* Laura N. Lowes, Nilanjan Mitra, and Arash Altoontash. February 2004.
- PEER 2003/09** *Sequencing Repairs after an Earthquake: An Economic Approach.* Marco Casari and Simon J. Wilkie. April 2004.
- PEER 2003/08** *A Technical Framework for Probability-Based Demand and Capacity Factor Design (DCFD) Seismic Formats.* Fatemeh Jalayer and C. Allin Cornell. November 2003.
- PEER 2003/07** *Uncertainty Specification and Propagation for Loss Estimation Using FOSM Methods.* Jack W. Baker and C. Allin Cornell. September 2003.
- PEER 2003/06** *Performance of Circular Reinforced Concrete Bridge Columns under Bidirectional Earthquake Loading.* Mahmoud M. Hachem, Stephen A. Mahin, and Jack P. Moehle. February 2003.

- PEER 2003/05** *Response Assessment for Building-Specific Loss Estimation.* Eduardo Miranda and Shahram Taghavi. September 2003.
- PEER 2003/04** *Experimental Assessment of Columns with Short Lap Splices Subjected to Cyclic Loads.* Murat Melek, John W. Wallace, and Joel Conte. April 2003.
- PEER 2003/03** *Probabilistic Response Assessment for Building-Specific Loss Estimation.* Eduardo Miranda and Hesameddin Aslani. September 2003.
- PEER 2003/02** *Software Framework for Collaborative Development of Nonlinear Dynamic Analysis Program.* Jun Peng and Kincho H. Law. September 2003.
- PEER 2003/01** *Shake Table Tests and Analytical Studies on the Gravity Load Collapse of Reinforced Concrete Frames.* Kenneth John Elwood and Jack P. Moehle. November 2003.
- PEER 2002/24** *Performance of Beam to Column Bridge Joints Subjected to a Large Velocity Pulse.* Natalie Gibson, André Filiatrault, and Scott A. Ashford. April 2002.
- PEER 2002/23** *Effects of Large Velocity Pulses on Reinforced Concrete Bridge Columns.* Greg L. Orozco and Scott A. Ashford. April 2002.
- PEER 2002/22** *Characterization of Large Velocity Pulses for Laboratory Testing.* Kenneth E. Cox and Scott A. Ashford. April 2002.
- PEER 2002/21** *Fourth U.S.-Japan Workshop on Performance-Based Earthquake Engineering Methodology for Reinforced Concrete Building Structures.* December 2002.
- PEER 2002/20** *Barriers to Adoption and Implementation of PBEE Innovations.* Peter J. May. August 2002.
- PEER 2002/19** *Economic-Engineered Integrated Models for Earthquakes: Socioeconomic Impacts.* Peter Gordon, James E. Moore II, and Harry W. Richardson. July 2002.
- PEER 2002/18** *Assessment of Reinforced Concrete Building Exterior Joints with Substandard Details.* Chris P. Pantelides, Jon Hansen, Justin Nadauld, and Lawrence D. Reaveley. May 2002.
- PEER 2002/17** *Structural Characterization and Seismic Response Analysis of a Highway Overcrossing Equipped with Elastomeric Bearings and Fluid Dampers: A Case Study.* Nicos Makris and Jian Zhang. November 2002.
- PEER 2002/16** *Estimation of Uncertainty in Geotechnical Properties for Performance-Based Earthquake Engineering.* Allen L. Jones, Steven L. Kramer, and Pedro Arduino. December 2002.
- PEER 2002/15** *Seismic Behavior of Bridge Columns Subjected to Various Loading Patterns.* Asadollah Esmaeily-Gh. and Yan Xiao. December 2002.
- PEER 2002/14** *Inelastic Seismic Response of Extended Pile Shaft Supported Bridge Structures.* T.C. Hutchinson, R.W. Boulanger, Y.H. Chai, and I.M. Idriss. December 2002.
- PEER 2002/13** *Probabilistic Models and Fragility Estimates for Bridge Components and Systems.* Paolo Gardoni, Armen Der Kiureghian, and Khalid M. Mosalam. June 2002.
- PEER 2002/12** *Effects of Fault Dip and Slip Rake on Near-Source Ground Motions: Why Chi-Chi Was a Relatively Mild M7.6 Earthquake.* Brad T. Aagaard, John F. Hall, and Thomas H. Heaton. December 2002.
- PEER 2002/11** *Analytical and Experimental Study of Fiber-Reinforced Strip Isolators.* James M. Kelly and Shakhzod M. Takhirov. September 2002.
- PEER 2002/10** *Centrifuge Modeling of Settlement and Lateral Spreading with Comparisons to Numerical Analyses.* Sivapalan Gajan and Bruce L. Kutter. January 2003.
- PEER 2002/09** *Documentation and Analysis of Field Case Histories of Seismic Compression during the 1994 Northridge, California, Earthquake.* Jonathan P. Stewart, Patrick M. Smith, Daniel H. Whang, and Jonathan D. Bray. October 2002.
- PEER 2002/08** *Component Testing, Stability Analysis and Characterization of Buckling-Restrained Unbonded BracesTM.* Cameron Black, Nicos Makris, and Ian Aiken. September 2002.
- PEER 2002/07** *Seismic Performance of Pile-Wharf Connections.* Charles W. Roeder, Robert Graff, Jennifer Soderstrom, and Jun Han Yoo. December 2001.
- PEER 2002/06** *The Use of Benefit-Cost Analysis for Evaluation of Performance-Based Earthquake Engineering Decisions.* Richard O. Zerbe and Anthony Falit-Baiamonte. September 2001.
- PEER 2002/05** *Guidelines, Specifications, and Seismic Performance Characterization of Nonstructural Building Components and Equipment.* André Filiatrault, Constantin Christopoulos, and Christopher Stearns. September 2001.

- PEER 2002/04** *Consortium of Organizations for Strong-Motion Observation Systems and the Pacific Earthquake Engineering Research Center Lifelines Program: Invited Workshop on Archiving and Web Dissemination of Geotechnical Data, 4–5 October 2001.* September 2002.
- PEER 2002/03** *Investigation of Sensitivity of Building Loss Estimates to Major Uncertain Variables for the Van Nuys Testbed.* Keith A. Porter, James L. Beck, and Rustem V. Shaikhutdinov. August 2002.
- PEER 2002/02** *The Third U.S.-Japan Workshop on Performance-Based Earthquake Engineering Methodology for Reinforced Concrete Building Structures.* July 2002.
- PEER 2002/01** *Nonstructural Loss Estimation: The UC Berkeley Case Study.* Mary C. Comerio and John C. Stallmeyer. December 2001.
- PEER 2001/16** *Statistics of SDF-System Estimate of Roof Displacement for Pushover Analysis of Buildings.* Anil K. Chopra, Rakesh K. Goel, and Chatpan Chintanapakdee. December 2001.
- PEER 2001/15** *Damage to Bridges during the 2001 Nisqually Earthquake.* R. Tyler Ranf, Marc O. Eberhard, and Michael P. Berry. November 2001.
- PEER 2001/14** *Rocking Response of Equipment Anchored to a Base Foundation.* Nicos Makris and Cameron J. Black. September 2001.
- PEER 2001/13** *Modeling Soil Liquefaction Hazards for Performance-Based Earthquake Engineering.* Steven L. Kramer and Ahmed-W. Elgamal. February 2001.
- PEER 2001/12** *Development of Geotechnical Capabilities in OpenSees.* Boris Jeremi . September 2001.
- PEER 2001/11** *Analytical and Experimental Study of Fiber-Reinforced Elastomeric Isolators.* James M. Kelly and Shakhzod M. Takhirov. September 2001.
- PEER 2001/10** *Amplification Factors for Spectral Acceleration in Active Regions.* Jonathan P. Stewart, Andrew H. Liu, Yoojoong Choi, and Mehmet B. Baturay. December 2001.
- PEER 2001/09** *Ground Motion Evaluation Procedures for Performance-Based Design.* Jonathan P. Stewart, Shyh-Jeng Chiou, Jonathan D. Bray, Robert W. Graves, Paul G. Somerville, and Norman A. Abrahamson. September 2001.
- PEER 2001/08** *Experimental and Computational Evaluation of Reinforced Concrete Bridge Beam-Column Connections for Seismic Performance.* Clay J. Naito, Jack P. Moehle, and Khalid M. Mosalam. November 2001.
- PEER 2001/07** *The Rocking Spectrum and the Shortcomings of Design Guidelines.* Nicos Makris and Dimitrios Konstantinidis. August 2001.
- PEER 2001/06** *Development of an Electrical Substation Equipment Performance Database for Evaluation of Equipment Fragilities.* Thalia Agnanos. April 1999.
- PEER 2001/05** *Stiffness Analysis of Fiber-Reinforced Elastomeric Isolators.* Hsiang-Chuan Tsai and James M. Kelly. May 2001.
- PEER 2001/04** *Organizational and Societal Considerations for Performance-Based Earthquake Engineering.* Peter J. May. April 2001.
- PEER 2001/03** *A Modal Pushover Analysis Procedure to Estimate Seismic Demands for Buildings: Theory and Preliminary Evaluation.* Anil K. Chopra and Rakesh K. Goel. January 2001.
- PEER 2001/02** *Seismic Response Analysis of Highway Overcrossings Including Soil-Structure Interaction.* Jian Zhang and Nicos Makris. March 2001.
- PEER 2001/01** *Experimental Study of Large Seismic Steel Beam-to-Column Connections.* Egor P. Popov and Shakhzod M. Takhirov. November 2000.
- PEER 2000/10** *The Second U.S.-Japan Workshop on Performance-Based Earthquake Engineering Methodology for Reinforced Concrete Building Structures.* March 2000.
- PEER 2000/09** *Structural Engineering Reconnaissance of the August 17, 1999 Earthquake: Kocaeli (Izmit), Turkey.* Halil Sezen, Kenneth J. Elwood, Andrew S. Whittaker, Khalid Mosalam, John J. Wallace, and John F. Stanton. December 2000.
- PEER 2000/08** *Behavior of Reinforced Concrete Bridge Columns Having Varying Aspect Ratios and Varying Lengths of Confinement.* Anthony J. Calderone, Dawn E. Lehman, and Jack P. Moehle. January 2001.
- PEER 2000/07** *Cover-Plate and Flange-Plate Reinforced Steel Moment-Resisting Connections.* Taejin Kim, Andrew S. Whittaker, Amir S. Gilani, Vitelmo V. Bertero, and Shakhzod M. Takhirov. September 2000.
- PEER 2000/06** *Seismic Evaluation and Analysis of 230-kV Disconnect Switches.* Amir S. J. Gilani, Andrew S. Whittaker, Gregory L. Fenves, Chun-Hao Chen, Henry Ho, and Eric Fujisaki. July 2000.

- PEER 2000/05** *Performance-Based Evaluation of Exterior Reinforced Concrete Building Joints for Seismic Excitation.* Chandra Clyde, Chris P. Pantelides, and Lawrence D. Reaveley. July 2000.
- PEER 2000/04** *An Evaluation of Seismic Energy Demand: An Attenuation Approach.* Chung-Che Chou and Chia-Ming Uang. July 1999.
- PEER 2000/03** *Framing Earthquake Retrofitting Decisions: The Case of Hillside Homes in Los Angeles.* Detlof von Winterfeldt, Nels Roselund, and Alicia Kitsuse. March 2000.
- PEER 2000/02** *U.S.-Japan Workshop on the Effects of Near-Field Earthquake Shaking.* Andrew Whittaker, ed. July 2000.
- PEER 2000/01** *Further Studies on Seismic Interaction in Interconnected Electrical Substation Equipment.* Armen Der Kiureghian, Kee-Jeung Hong, and Jerome L. Sackman. November 1999.
- PEER 1999/14** *Seismic Evaluation and Retrofit of 230-kV Porcelain Transformer Bushings.* Amir S. Gilani, Andrew S. Whittaker, Gregory L. Fenves, and Eric Fujisaki. December 1999.
- PEER 1999/13** *Building Vulnerability Studies: Modeling and Evaluation of Tilt-up and Steel Reinforced Concrete Buildings.* John W. Wallace, Jonathan P. Stewart, and Andrew S. Whittaker, editors. December 1999.
- PEER 1999/12** *Rehabilitation of Nonductile RC Frame Building Using Encasement Plates and Energy-Dissipating Devices.* Mehrdad Sasani, Vitelmo V. Bertero, James C. Anderson. December 1999.
- PEER 1999/11** *Performance Evaluation Database for Concrete Bridge Components and Systems under Simulated Seismic Loads.* Yael D. Hose and Frieder Seible. November 1999.
- PEER 1999/10** *U.S.-Japan Workshop on Performance-Based Earthquake Engineering Methodology for Reinforced Concrete Building Structures.* December 1999.
- PEER 1999/09** *Performance Improvement of Long Period Building Structures Subjected to Severe Pulse-Type Ground Motions.* James C. Anderson, Vitelmo V. Bertero, and Raul Bertero. October 1999.
- PEER 1999/08** *Envelopes for Seismic Response Vectors.* Charles Menun and Armen Der Kiureghian. July 1999.
- PEER 1999/07** *Documentation of Strengths and Weaknesses of Current Computer Analysis Methods for Seismic Performance of Reinforced Concrete Members.* William F. Cofer. November 1999.
- PEER 1999/06** *Rocking Response and Overturning of Anchored Equipment under Seismic Excitations.* Nicos Makris and Jian Zhang. November 1999.
- PEER 1999/05** *Seismic Evaluation of 550 kV Porcelain Transformer Bushings.* Amir S. Gilani, Andrew S. Whittaker, Gregory L. Fenves, and Eric Fujisaki. October 1999.
- PEER 1999/04** *Adoption and Enforcement of Earthquake Risk-Reduction Measures.* Peter J. May, Raymond J. Burby, T. Jens Feeley, and Robert Wood.
- PEER 1999/03** *Task 3 Characterization of Site Response General Site Categories.* Adrian Rodriguez-Marek, Jonathan D. Bray, and Norman Abrahamson. February 1999.
- PEER 1999/02** *Capacity-Demand-Diagram Methods for Estimating Seismic Deformation of Inelastic Structures: SDF Systems.* Anil K. Chopra and Rakesh Goel. April 1999.
- PEER 1999/01** *Interaction in Interconnected Electrical Substation Equipment Subjected to Earthquake Ground Motions.* Armen Der Kiureghian, Jerome L. Sackman, and Kee-Jeung Hong. February 1999.
- PEER 1998/08** *Behavior and Failure Analysis of a Multiple-Frame Highway Bridge in the 1994 Northridge Earthquake.* Gregory L. Fenves and Michael Ellery. December 1998.
- PEER 1998/07** *Empirical Evaluation of Inertial Soil-Structure Interaction Effects.* Jonathan P. Stewart, Raymond B. Seed, and Gregory L. Fenves. November 1998.
- PEER 1998/06** *Effect of Damping Mechanisms on the Response of Seismic Isolated Structures.* Nicos Makris and Shih-Po Chang. November 1998.
- PEER 1998/05** *Rocking Response and Overturning of Equipment under Horizontal Pulse-Type Motions.* Nicos Makris and Yiannis Roussos. October 1998.
- PEER 1998/04** *Pacific Earthquake Engineering Research Invitational Workshop Proceedings, May 14-15, 1998: Defining the Links between Planning, Policy Analysis, Economics and Earthquake Engineering.* Mary Comerio and Peter Gordon. September 1998.
- PEER 1998/03** *Repair/Upgrade Procedures for Welded Beam to Column Connections.* James C. Anderson and Xiaojing Duan. May 1998.
- PEER 1998/02** *Seismic Evaluation of 196 kV Porcelain Transformer Bushings.* Amir S. Gilani, Juan W. Chavez, Gregory L. Fenves, and Andrew S. Whittaker. May 1998.

PEER 1998/01 *Seismic Performance of Well-Confined Concrete Bridge Columns.* Dawn E. Lehman and Jack P. Moehle.
December 2000.

ONLINE REPORTS

The following PEER reports are available by Internet only at http://peer.berkeley.edu/publications/peer_reports.html

- PEER 2009/105** *Reduced Uncertainty of Ground Motion Prediction Equations through Bayesian Variance Analysis.* Robb Eric S. Moss. November 2009.
- PEER 2009/104** *Advanced Implementation of Hybrid Simulation.* Andreas H. Schellenberg, Stephen A. Mahin, Gregory L. Fenves. November 2009.
- PEER 2009/103** *Performance Evaluation of Innovative Steel Braced Frames.* T. Y. Yang, Jack P. Moehle, and Božidar Stojadinović. August 2009.
- PEER 2009/102** *Reinvestigation of Liquefaction and Nonliquefaction Case Histories from the 1976 Tangshan Earthquake.* Robb Eric Moss, Robert E. Kayen, Liyuan Tong, Songyu Liu, Guojun Cai, and Jiaer Wu. August 2009.
- PEER 2009/101** *Report of the First Joint Planning Meeting for the Second Phase of NEES/E-Defense Collaborative Research on Earthquake Engineering.* Stephen A. Mahin et al. July 2009.
- PEER 2008/104** *Experimental and Analytical Study of the Seismic Performance of Retaining Structures.* Linda Al Atik and Nicholas Sitar. January 2009.
- PEER 2008/103** *Experimental and Computational Evaluation of Current and Innovative In-Span Hinge Details in Reinforced Concrete Box-Girder Bridges. Part 1: Experimental Findings and Pre-Test Analysis.* Matias A. Hube and Khalid M. Mosalam. January 2009.
- PEER 2008/102** *Modeling of Unreinforced Masonry Infill Walls Considering In-Plane and Out-of-Plane Interaction.* Stephen Kadysiewski and Khalid M. Mosalam. January 2009.
- PEER 2008/101** *Seismic Performance Objectives for Tall Buildings.* William T. Holmes, Charles Kircher, William Petak, and Nabih Youssef. August 2008.
- PEER 2007/101** *Generalized Hybrid Simulation Framework for Structural Systems Subjected to Seismic Loading.* Tarek Elkhoraibi and Khalid M. Mosalam. July 2007.
- PEER 2007/100** *Seismic Evaluation of Reinforced Concrete Buildings Including Effects of Masonry Infill Walls.* Alidad Hashemi and Khalid M. Mosalam. July 2007.